THE DEVELOPMENT OF AN OPTIMIZED GENERATOR PRODUCTION

METHOD FOR THE ROUTINE PRODUCTION OF ZINC-62/COPPER-62

GENERATOR SYSTEMS

A Thesis

by

TYLER LEE CANTRELL

Submitted to the Office of Graduate Studies and Professional Studies of
Texas A&M University
in partial fulfillment of the requirements for the degree of

MASTER OF SCIENCE

Chair of Committee,	Gamal Akabani
Committee Members,	Craig Marianno
	Charles M. Folden III
Head of Department,	Yassin Hassan

May 2015

Major Subject: Health Physics

ABSTRACT

The demand for radionuclides used in positron emission tomography (PET) must

be met if the role for PET in Nuclear Medicine is to be expanded. The best method for

supplying PET radionuclides to satellite PET facilities is through the use of radionuclide

generators. The generator of interest in this study was the ^{62}Zn/^{62}Cu generator system.

The objective of this study was to optimize the methods for producing ^{62}Zn/^{62}Cu so that

they may be better suited for routine production. This involved examination of the

bombardment parameters and the procedure utilized to dissolve the irradiated copper

target. Additionally, the feasibility in automating the different processes of the

production methods through a modular system was examined to aid in streamlining the

routine production of the generator systems.

The analysis showed that, between proton entry energies of 18 and 30 MeV, a

target thickness of 1.0 mm was optimal for producing ^{62}Zn. With a 1.0 mm thick target,

the optimal proton entry energy for maximizing the production yield of ^{62}Zn was 29

MeV. The theoretical ^{62}Zn yield at 29 MeV directly prior to generator loading was

calculated to be between 160 and 180 GBq·μA^{-1}·h^{-1}. An alternative target processing

method based on 30% hydrogen peroxide (H$_2$O$_2$) and 2 M hydrochloric acid (HCl) at a

temperature of 75 °C successfully dissolved the copper foil within 12 minutes. The color

of the solution indicated that the copper (II) ions formed the hexaaquacopper(II) ion in 2

M HCl used for chemical separation. Finally, devices were purchased for automating the

generator production process, including heating and transfer of solutions, and electronic

manipulation of valves. These devices were controlled using the software LabVIEW

which demonstrated the feasibility of building a system capable of automating the

production of this generator system. A detailed overview was provided on how to

control these instruments with LabVIEW.

ACKNOWLEDGEMENTS

NOMENCLATURE

Bq	Becquerel
CAD	Coronary Artery Disease
CT	X-ray Computed Tomography
DV1	Dissolution Vessel 1
DV2	Dissolution Vessel 2
EOB	End of Bombardment
JANIS	Java-base Nuclear Data Information System
MRI	Magnetic Resonance Imaging
NIST	National Institute of Standards and Technology
PET	Positron Emission Tomography
SF	Saturation Factor, $(1 - e^{\lambda t})$
SRIM	The Stopping and Range of Ions in Matter

TABLE OF CONTENTS

LIST OF FIGURES

LIST OF TABLES

1. INTRODUCTION

1.1 PET Diagnostic Imaging

Positron Emission Tomography (PET) is one of the fastest growing diagnostic specialties in nuclear medicine (Bailey et al., 2005). PET is a nuclear diagnostic method that can quantitatively measure the physiological activities and chemical reactions occurring within specific regions of tissue or organs (Coleman, 1988; Green et al., 1990; Qaim, 2012; Schiepers and Hoh, 2006). This is accomplished with the use of a molecular probe or pharmaceutical compound labeled with a positron emitting radionuclide (Qaim, 2012). One of the most common examples of a molecular probe in PET imaging is the use of a glucose analogue, 2-^{18}F-fluoro-2-deoxy-D-glucose (FDG), labeled with the PET tracer ^{18}F to non-invasively measure glucose metabolism in tumors (Schiepers and Hoh, 2006). PET is useful not only for providing diagnostic imaging of existing disease but also for detecting disease in its earliest stages. Other imaging modalities such as computed tomography (CT) or magnetic resonance imaging (MRI) only provide anatomic information (Coleman, 1988). Generally, anatomic changes are only evident after the disease has manifested. PET is able to detect chemical changes in the form of functional abnormalities that occur prior to anatomic changes (Coleman, 1988). A few examples of functional abnormalities in diseases detectable by PET are epilepsy, Huntington's disease, and coronary artery disease (CAD) (Coleman, 1988).

Since its first acceptance for clinical use in the 1980's, PET imaging has significantly impacted patient management. The decisions on the surgical treatment for diseases are changing with the diagnostic information provided by PET imaging.

Inappropriate surgeries are avoided, curative resections are more likely, diagnosing and treating lymphoma is possible, diagnosis of patients at risk for CAD is possible, and surgical decisions with other types of disease can be greatly benefited with the use of PET imaging (Bailey et al., 2005). This level of patient care has not been achieved before by Nuclear Medicine (Bailey et al., 2005). PET imaging currently finds clinical applications primarily in Oncology, Cardiology, and Neuropsychiatry with focuses in cancer diagnosis/management, cardiac surgery, and neurology/psychiatry, respectively (Bailey et al., 2005).

PET imaging is currently very powerful with the use of FDG, an effective and powerful radiopharmaceutical, but it also currently needs technical advancements before it starts achieving widespread use in Nuclear Medicine (Bailey et al., 2005). More sensitive PET instrumentation is being developed, significantly increasing patient throughput with shorter scanning times. The development of fusion imaging, the simultaneous use of PET with other imaging modalities, shows a promising new methodology. The spatial resolution of PET images are also improving, allowing for images down to a millimeter in resolution. All of the time and money being placed into these technical advancements and more are being driven by an industry who believes that PET imaging is a worthwhile area of expansion (Bailey et al., 2005). As PET imaging continues to grow, there will be increasing opportunities for studies to be conducted with PET radionuclides. The increase in demands for PET radionuclides will have to be met by cyclotron operators and radiochemists who are the sole source of PET radionuclides.

1.2   Common Radionuclides Used in PET

PET radionuclide can only be produced at a cyclotron facility. There are a large

number of positron-emitting radionuclides available for production but very few actually

fit the requirements of a PET radionuclide. The underlying principle behind diagnostic

nuclear medicine is to deliver as little radiation dose to the patient as possible while

maintaining the desired quality of the image (Qaim, 2011). This requires that the

radionuclide have a short half-life, emit low energy positrons, and have zero high-energy

gamma-ray emissions (Qaim, 2012). The other consideration when picking a PET

radionuclide is its usability as a radiopharmaceutical. Creating a radiopharmaceutical

labeled with a PET tracer and utilizing the same compound in a PET study does not

always work together. At the end of synthesis, the labeled compound often doesn't have

the level of activity necessary to conduct a PET study, as a result, a major consideration

of a PET radionuclide is the time required to complete the

synthesis, purification, and sterilization of the final radiopharmaceutical product

(Yamamoto, 1984).

The most common PET radionuclides are ^{18}F ($T_{1/2}$ = 110 min) and certain

organic analogues of natural body constituents such as ^{11}C ($T_{1/2}$ = 20.4 min), ^{13}N ($T_{1/2}$ =

10 min), and ^{15}O ($T_{1/2}$ = 2 min) (Green et al., 1990; Qaim, 2012; Robinson Jr et al.,

1980; Yamamoto, 1984). The radionuclides ^{11}C, ^{13}N, and ^{15}O have such short half-lives

that they must be produced with an in-house cyclotron and processed on site. Even in the

cases where in-house cyclotrons are available, their available labeled compounds are

limited due to their short half-lives. With a longer half-life, ^{18}F can be used at facilities

3

located within 2 hours of a cyclotron facility (Yamamoto, 1984). Table 1 lists the most common PET radionuclides and Table 2 lists several radiopharmaceuticals and their applications with these PET radionuclides.

In recent years, efforts have been extended towards the development of novel or non-standard positron emitters. This is due to the growing significance of PET in diagnostic nuclear medicine which has manifested in a growing demand for positron emitters that have different and more specialized applications than the common PET radionuclides in Table 1 (Qaim, 2012). To be viable, the novel positron emitters must be producible in a cyclotron with a high degree of yield and radionuclide purity as well as contain the desired decay characteristics for suitable imaging (Qaim, 2011).

Table 1. Short list of common positron emitters used for PET imaging (Qaim, 2012).

Positron Emitters for PET			
Radionuclide	Half-life (min)	Radiation Emitted	Production Process
^{11}C	20.4	β+	^{14}N(p,α)
^{13}N	10	β+	^{16}O(p,α)
^{15}O	2	β+	^{14}N(d,n) ^{15}N(p,n)
^{18}F	110	β+	^{18}O(p,n) ^{20}Ne(d,α)
^{68}Ga	68.3	β+	^{69}Ga(p,2n)^{68}Ge (generator)
^{82}Rb	1.3	β+	^{nat}Rb(p,x)^{82}Sr (generator)

Table 2. List of positron labelled radiopharmaceuticals for PET (Yamamoto, 1984).

Radiopharmaceuticals	Primary Applications
^{15}O-H_2O, ^{15}O-CO_2, ^{18}F-CH_3F, ^{18}F-antipyrine, ^{11}C-alcohols, ^{15}O-N_2O	Cerebral blood flow
^{11}C-CO, ^{15}O-CO	Cerebral blood volume
^{15}O-O_2	Cerebral oxygen utilization
^{18}F-2-FDG, ^{11}C-2-DG, ^{11}C-glucose	Glucose utilization
^{11}C-labelled; L-leucine, L-valine, L-methionine	Protein syntheses
^{11}C-3-O-methyl-D-glucose	Glucose transport
^{18}F- and ^{11}C-spiroperidol, ^{75}Br-bromo-spiroperidol, ^{18}F-haloperidol, ^{11}C-pimozide	Dopaminergic receptors
^{18}F-L-DOPA	Neurotransmitter
^{11}C- and ^{13}N-BCNU	Pharmacokinetics

1.3   Initial and Operational Cost

There are two major components that comprise the cost of utilizing PET imaging that have been cost-prohibitive towards the wider implementation of PET imaging. The first component is the capital cost to purchase and field a cyclotron facility and its staff. The second is the capital cost for purchasing a high-resolution PET imaging equipment. In 1988, a review was conducted on the clinical status of PET in the United States and it found that the cost of PET scanners ranged from $1.0 to $1.8 million. The cost to obtain a medium energy cyclotron ranged from $1.0 to $2.0 million with an estimated additional annual operating cost of $0.4 to $1.0 million (Coleman, 1988).

Currently, there are two cyclotron vendors, IBA Technology Group in Belgium and Advanced Cyclotron Systems, Inc. in Canada, which have the capability to produce medium to high-energy cyclotrons. Advanced Cyclotron Systems, Inc. reports that its

current TR-24 model Cyclotron, 18-24 MeV, has an estimated cost between $2.0 and $4.0 million, including building the facility, and $50k to $300k in maintenance and operational annual cost. More recently, the price of PET scanners have remained within the $2.2 million range and can fluctuate according to the image quality desired (Keppler and Conti, 2001). Given this, it can be shown that the financial burden associated with building and fielding both of these facilities has remained consistent over the past 30 years.

The routine cost for PET scanning, assuming an average of 12 doses per day, ranges between $900 and $1,500. This involves the use of FDG for whole body, brain, and cardiac perfusion imaging. The routine cost for producing radiopharmaceuticals, again with an average of 12 doses per day, ranges between $700 and $1,452 (Keppler and Conti, 2001). The variation in routine costs are associated with the type of facility configuration being used where the most expensive item is the use of one cyclotron to support a single scanning facility and the least expensive being the use of a satellite scanning facility that purchases radiopharmaceuticals (Keppler and Conti, 2001). This indicates that the most financially viable option for utilizing PET imaging, given the start-up/operational costs of fielding an in-house cyclotron and scanning facility, is the use of a scanning facility that can purchase PET radionuclides from a remote manufacturer.

1.4   PET Radionuclide Generators

One of the most commonly utilized PET radiopharmaceuticals, FDG, is extremely limited in its range of shipment from a cyclotron facility due to its 110 min half-life. Other PET radionuclides are simply impossible to ship due to their very short half-life. The answer to the effective distribution of short-lived PET radionuclides is the use of generator systems (Lebowitz and Richards, 1974). The ability to obtain a PET radionuclide from a parent/daughter generator system would effectively increase the distribution range of a cyclotron facility, making PET imaging available on a much broader scale (Fujibayashi, 1989; Green et al., 1990; Mathias et al., 1990; Zweit et al., 1992).

A generator system is composed of a parent radionuclide, with a relatively long half-life, that decays to the desired daughter PET radionuclide. The separation and extraction of the daughter PET radionuclide from the parent is based upon their chemical differences most easily exploited through the use of a column chromatograph. This ion separation technique provides an extremely high chemical, radiochemical, and radionuclide purity making generator systems an ideal source of PET radionuclides for remote facilities (Lebowitz and Richards, 1974). Their rugged and compact design (Lebowitz and Richards, 1974) also makes it economically feasible for cyclotron facilities to distribute these generators to remote facilities.

However, current standard PET radionuclide generator systems contain undesirable characteristics. The $^{82}Sr/^{82}Rb$ generator system requires spallation of molybdenum with 800 MeV protons (Bilewicz, 2006) in an accelerator to produce

sufficient quantities of ^{82}Sr (Lebowitz and Richards, 1974). The generator system can

also be produced by irradiating an ^{85}Rb target with protons that have energies greater

than 40 MeV. While the 76 second half-life of ^{82}Rb is very well suited for assessing

myocardial perfusion, its uses are limited due to the chemistry of the rubidium cation

(Beanlands et al., 1992; Green et al., 1988). The other available system, ^{68}Ge/^{68}Ga, can

be commercially produced with 20 MeV protons utilizing the reaction ^{69}Ga(p,2n)^{68}Ge.

This generator system has an ideal parent half-life of 271 days but a daughter half-life of

68 minutes. In many situations, the half-life of the daughter is sufficiently long that it

limits the uses of ^{68}Ge in clinical settings due to the levels of radiation dose delivered to

the patients (Robinson Jr et al., 1980). Given this, there are generator systems available

that can yield PET radionuclides, but these novel PET radionuclides are limited in their

applications similar to the common PET radionuclides. Attention must be directed

towards a novel positron emitter and its generator system that is produced cheaply by the

PET manufacturer, and has a wide range of implementation into different clinical

studies. Such a generator system that has the potential to meet both of these criteria is the

^{62}Zn/^{62}Cu generator.

1.5   The ^{62}Zn/^{62}Cu Generator

      ^{62}Zn is produced with the use of a medium energy cyclotron and has a half-life of

9.186 hours. It decays to ^{62}Cu ($T_{1/2} = 9.74$ min), which has a half-life well suited for the

time frame of PET perfusion imaging but remains sufficiently long-lived to allow its

incorporation in a diverse set of radiopharmaceuticals (Green et al., 1990; Mathias et al.,

1990). Copper has a very well understood chemistry and is dominated by two oxidation states I and II (Blower et al., 1996). This allows for, in many cases, easy manipulation of copper in aqueous solutions due to its flexible coordination chemistry (Smith and Martell, 1975).

The chemistry and half-life of ^{62}Cu makes it an extremely desirable PET radionuclide for pharmaceuticals (Fujibayashi, 1989). Previous studies have utilized ^{62}Cu labeled radiopharmaceuticals for different applications such as ^{62}Cu-PTSM for cerebral and myocardial PET perfusion imaging (Green, 1987; Green et al., 1988; Haynes et al., 2000; Mathias et al., 1990) and ^{62}Cu-DTS-HAS for regional plasma volume measurements (Fujibayashi, 1990). Studies on other possible ^{62}Cu labeled radiopharmaceuticals have been conducted as well (Yokoyama et al., 1986).

The radionuclide ^{62}Zn has a slight disadvantage with its short half-life, giving the generator system a shelf life of approximately 1 to 3 days (Blower et al., 1996; Haynes et al., 2000; Zweit et al., 1992). However, this is somewhat offset by the ability to produce ^{62}Zn with large production yields ranging between 2.6 (Robinson Jr et al., 1980) and 5.2 (Zweit et al., 1992) GBq. Ultimately, the shelf-life is trivial next to the estimated production cost of less than $500 dollar per unit (Haynes et al., 2000). Additionally, with a ^{62}Cu elution available every 30 to 45 minutes (Blower et al., 1996), the throughput potential for this generator system is very high, allowing for PET imaging to be conducted with a large number of patients regardless of the shelf-life (Keppler and Conti, 2001). The economic and clinically versatile characteristics of the ^{62}Zn/^{62}Cu generator system work in an advantageous manner towards establishing the existence of

9

satellite PET imaging centers (Mathias et al., 1990) and ultimately broadening the role of PET imaging in Nuclear Medicine.

1.5   Purpose

The ^{62}Zn/^{62}Cu generators are ideal for establishing satellite PET imaging facilities. The generator system has an economic and clinically versatile application within PET imaging, and can support PET to achieve a broader role in Nuclear Medicine. In addition to its advantageous applications, the generator system's production is very well characterized and defined. The ^{62}Zn reaction cross sections, cyclotron targetry, target processing, chemical processing, and generator loading procedure and methods are all well known. However, the generator systems true economic potential has yet to be realized through the means of mass production.

This is due in part to the large volumes of corrosive fumes generated during the target-processing phase where the target is dissolved with highly concentrated acids. The corrosive fumes are extremely damaging to manufacturing equipment, including hot cells, which makes it difficult to implement at radiochemistry facilities. The lack of mass production is also due in part to the fact that the generator system has been produced primarily by research institutions and has not been optimized for routine production. Lastly, there is no automated system that is capable of streamlining the routine production of the generator system. A semi-automated system has been reported previously (Fukumura, 2006) but lacks a true modular and fully automatic design that is controlled through a single interface.

Therefore, it is the goal of this study to provide the foundation for the mass-production of the ^{62}Zn/^{62}Cu generator system. This will be accomplished by 1) developing a noncorrosive target processing procedure, 2) optimizing the routine production of ^{62}Zn, and 3) developing a proof of concept that illustrates the feasibility in automating the specific processes of transferring liquids, heating solutions, and manipulating electronic valves under current Good Manufacturing Practices (cGMP) conditions (21CFR212).

2. EXPERIMENTAL METHODS AND MATERIALS

2.1   The Radionuclides ^{62}Zn and ^{62}Cu

The radionuclide ^{62}Zn is a man-made radioisotope with a half-life of 9.186 h that decays to ^{62}Cu primarily via β^+ decay. The radionuclide ^{62}Cu has a half-life of 9.74 m and decays primarily via β^+ decay to stable ^{62}Ni. The decay scheme for ^{62}Zn is illustrated by Figure. 1. The radiative emissions for both ^{62}Zn and ^{62}Cu can be found in Tables 3 and 4. The symbols β^+ and ε represent positron decay and electron capture, respectively. All nuclear data were obtained from the National Nuclear Data Center's (NNDC) Nuclear structure and Decay data (NuDat) database.

Table 3. The radioactive decay data for ^{62}Zn represented by the energy, intensity, and decay mode of each radiative emission.

Emission	Intensity (%)	Energy (keV)
β^+	8.2	255*
$\gamma^\pm$	16.4	511
γ	14.8	508
γ	15.3	548
γ	26.0	597

* represents the maximum beta particle energy released.

Table 4. The radioactive decay data for ^{62}Cu represented by the energy, intensity, and decay mode of each radiative emission.

Emission	Intensity (%)	Energy (keV)
β^+	97.60	1321*
$\gamma^\pm$	196.0	511
γ	0.15	876
γ	0.34	1173

* represents the maximum beta energy released.
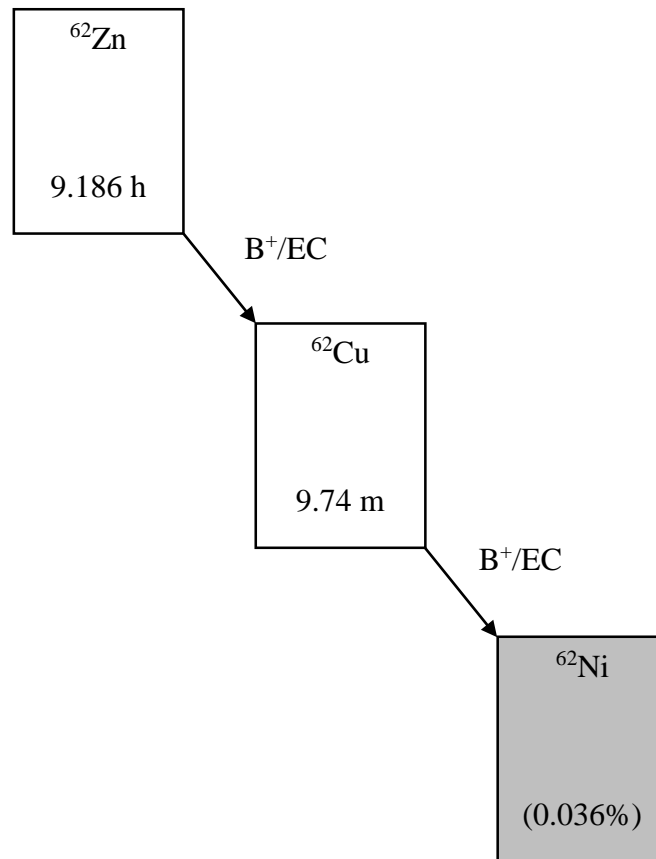
Figure 1. The decay scheme for ^{62}Zn, which decays by positron decay/electron capture to its daughter ^{62}Cu, which in turns decays via the same mechanism to stable ^{62}Ni.

2.2 Target Irradiation

2.2.1 Nuclear Reaction for Production of ^{62}Zn

The radionuclide ^{62}Zn can be produced via the nuclear reaction ^{nat}Cu(p,x)^{62}Zn by bombarding a natural copper target with protons (Grütter, 1982; Gul, 2001). This is the only viable nuclear reaction available for producing ^{62}Zn in a cyclotron. Copper has two naturally occurring isotopes of copper-63 and copper-65 with natural abundances of 69.17% and 30.83%, respectively. The specific nuclear reactions for each of the two isotopes that produce ^{62}Zn are ^{63}Cu(p,2n)^{62}Zn and ^{65}Cu(p,4n)^{62}Zn (Grütter, 1982; Gul, 2001). Due to this, both isotopes in natural copper will contribute towards the

13

production of ^{62}Zn. The reaction cross section for ^{62}Zn production with the two copper

isotopes as a function of proton energy is shown in Figure 2. The reaction

^{63}Cu(p,2n)^{62}Zn has a Q value of -13.265 MeV and a threshold production energy of

13.477 MeV and the cross sections peak at approximately 25 MeV. The reaction

^{65}Cu(p,4n)^{62}Zn has a Q value of -31.092 MeV and threshold production energy of

31.574 MeV and the cross sections peak at 45 MeV. Of these two open channels, the

former has a significantly higher cross section for producing ^{62}Zn at lower proton

energies. For this reason the nuclear reaction favored for producing ^{62}Zn is

^{63}Cu(p,2n)^{62}Zn, which is the most commonly utilized reaction in previous publications

(Blower et al., 1996; Fujibayashi, 1989; Fukumura, 2006; Haynes et al., 2000; Robinson

Jr et al., 1980; Zweit et al., 1992). A consequence of this is that ^{65}Cu is not utilized for

^{62}Zn production because the threshold for its nuclear reaction is above the energy used

for the ^{63}Cu nuclear reaction.
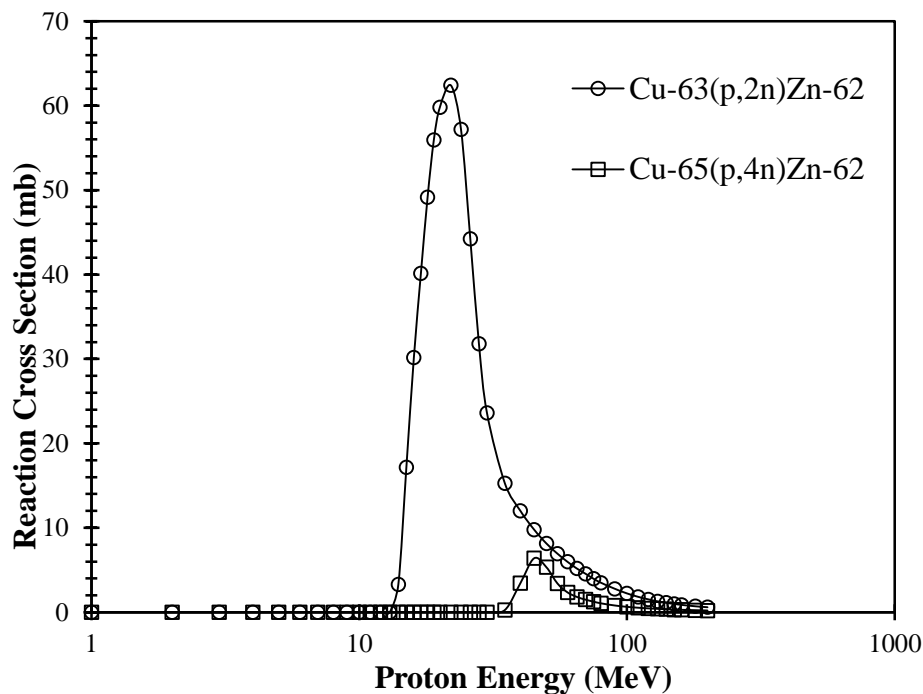
Figure 2. The reaction cross section for ^{62}Zn production via the isotopes copper-63 and copper-65, taken from JANIS (Soppera et al., 2014).

2.2.2   Nuclear Reactions For Production of Contaminants

Both isotopes, ^{63}Cu (69.15% natural abundance) and ^{65}Cu (30.85% natural abundance), contribute to the production of contaminants or unwanted radioactive isotopes during irradiation through a variety of ^{nat}Cu(p,x) nuclear reactions. A summary of each nuclear reaction, resulting contaminants, corresponding half-life, and daughter products is shown in Table 5.

Table 5. The contaminants produced from the nuclear reaction $^{nat}Cu(p,x)$ during the proton irradiation of a natural copper target (Soppera et al., 2014).

Target Isotope	Nuclear Reaction	Contaminant	Radioactive Half-life	Daughter Product
^{63}Cu	p,n	Zn-63	38.47 min	Cu-63
	p,3n	Zn-61	89.1 s	Cu-61
	p,2n+p	Cu-61	3.33 h	Ni-61
	p,n+p+a	Co-58	70.86 d	Fe-58
	p,γ	Zn-64	Stable	-
	p,p	Cu-63	Stable	-
	p,α	Ni-60	Stable	-
^{65}Cu	p,n	Zn-65	243.6 d	Cu-65
	p,3n	Zn-63	38.47 min	Cu-63
	p,n+p	Cu-64	12.7 h	Ni-64/Zn-64
	p,γ	Zn-66	Stable	-
	p,p	Cu-65	Stable	-
	p,α	Ni-62	Stable	-

2.2.3   Ideal Proton Energy Range

In practice, producing the highest specific activity of ^{62}Zn while minimizing impurities is the main goal when selecting the appropriate proton beam energy. This requires simultaneous consideration of the reaction cross-section for ^{62}Zn and of other contaminants (Table 5) because different quantities of each can be produced at the same proton energies. Figures 3 and 4 show all of the possible $^{63}Cu(p,x)$ and $^{65}Cu(p,x)$ nuclear reactions (Table 5), respectively, for proton energies between 1 and 200 MeV

16
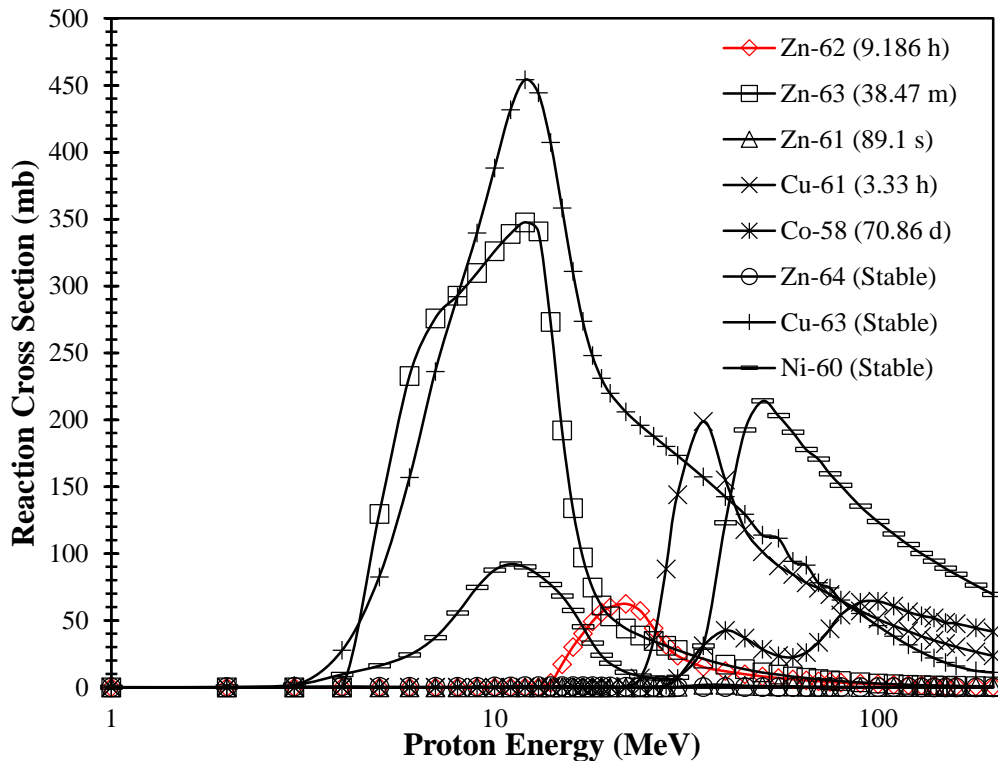
Figure 3. Reaction cross sections taken from JANIS (Soppera et al., 2014) of all possible nuclear reactions for protons bombarding ^{63}Cu with energies between 1 and 200 MeV.

Given the cross section data in Figures 3 and 4, it was determined that the ideal proton energy for maximizing the ^{62}Zn production yield with a high radionuclide purity would be between 18 and 30 MeV. Within this energy range several important contaminants reaction probability cross-sections are minimized. The copper contaminant ^{61}Cu ($T_{1/2} = 3.33$ h) has a maximum possible reaction cross-section of 199 mb at a proton energy of 35 MeV. With a proton entry energy of 30 MeV, the maximum possible reaction cross-section for ^{61}Cu is 144 mb. This value drops to less than 0.01 mb at a proton entry energy of 18 MeV. Thus, the production of ^{61}Cu is minimized as effectively as possible with proton entry energies between 18 and 30 MeV.
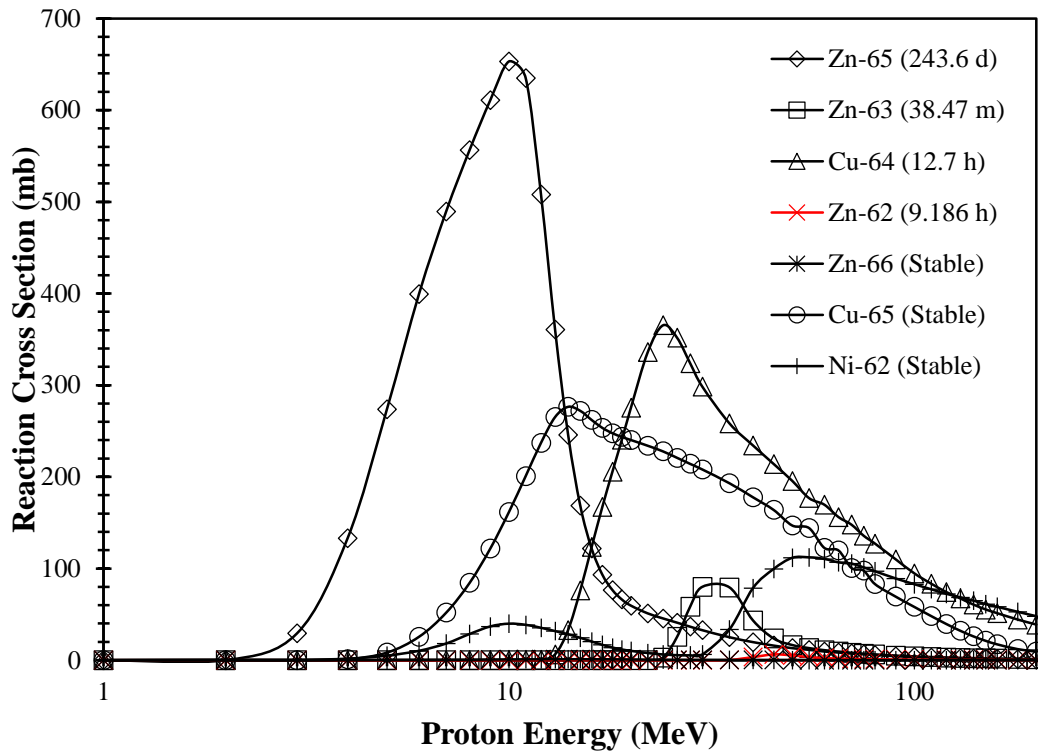
Figure 4. Reaction cross sections taken from JANIS (Soppera et al., 2014) of all possible nuclear reactions for protons bombarding ^{65}Cu with energies between 1 and 200 MeV.

Additionally, the other copper contaminant ^{64}Cu ($T_{1/2}$ = 12.7 h) has a maximum reaction cross-section of 365 mb at a proton energy of 24 MeV. While the production of this contaminant is not effectively minimized between proton entry energies of 18 and 30 MeV, ^{64}Cu only emits one gamma-ray with an emission rate of 0.5% and can be separated during the chemical processing phase. Thus, ^{64}Cu has a negligible impact on the radionuclide purity and presents itself as a negligible external radiological hazard.

The zinc contaminant ^{63}Zn ($T_{1/2}$ = 38.47 m) is produced through reactions with both natural copper isotopes in the target. With ^{63}Cu, the maximum ^{63}Zn reaction cross-section is 348 mb at a proton entry energy of 12 MeV. With the other copper isotope

^{65}Cu, the maximum ^{63}Zn reaction cross-section is 80 mb at proton entry energy of 30 MeV. Thus, between the proton entry energies of 18 and 30 MeV, the ^{63}Zn reaction cross-section is minimized between 74 and 100 mb through both natural copper isotopes. ^{63}Zn does not significantly affect the radionuclide purity of ^{62}Zn due to its short half-life, but can present an external radiological hazard following end of bombardment. Additionally, ^{61}Zn ($T_{1/2}$ = 89.1 s) is another short-lived zinc contaminant that is produced from ^{63}Cu. The production of this contaminant is negligible as it has a maximum reaction cross-section at 1.7 mb at a proton entry energy of 40 MeV with a reaction cross-section of less than 0.3 mb between proton entry energies of 18 and 30 MeV.

The only zinc contaminant that could potentially affect the radionuclide purity of ^{62}Zn is ^{65}Zn ($T_{1/2}$ = 244 d) due to its long half-life. The chemical processing phase separates the contaminants from ^{62}Zn based upon their different chemical properties. The ^{65}Zn contaminant cannot be separated as a result because it shares the same chemistry properties as ^{62}Zn. This contaminant is produced from ^{65}Cu and has a maximum reaction cross-section of 652 mb at a proton entry energy of 10 MeV. Between proton entry energies of 18 and 30 MeV, the reaction cross-section for this contaminant is effectively minimized between 77 and 32 mb, respectively.

The contaminant ^{58}Co ($T_{1/2}$ = 70.86 d) is produced from ^{63}Cu but has a reaction cross-section of less than 0.2 mb between proton entry energies of 18 and 30 MeV. ^{58}Co represents a negligible external radiological hazard and can be separated during chemical processing under the same reasoning listed for the separation of the other contaminants. Other stable isotopes produced are ^{60}Ni, ^{62}Ni, ^{64}Zn, ^{63}Cu, ^{66}Zn, and ^{65}Cu. These stable

isotopes are not an external radiological hazard and can be separated during the chemical processing phase. As a result, they do not impact the production yield or radionuclide purity of the final ^{62}Zn product.

2.2.4   Modeling Isotope Production Rate

The isotope production rate was modeled as a method of determining which proton energy maximized the production of ^{62}Zn. The production rate of an isotope can be defined as the number of nuclei i being formed per second minus the number of nuclei i decaying per second. This relationship takes the form of a differential equation that relates the gain and loss of nuclei i during production through various parameters seen in Equation 1 (Agency, 2009b).

$$A = \frac{N_A}{A_T} I (1 - e^{-\lambda t}) \int_{E_f}^{E_i} \frac{\sigma(E)}{S(E)} dE \tag{1}$$

where

I is the incident particle flux (s^{-1})
N_A is Avogadro's Number (nuclei·mol^{-1})
A_T is the molar mass of the material (g·mol^{-1})
λ is the decay constant of the product (s^{-1})
t is the bombardment time (s)
σ is the reaction cross-section and is a function of energy (cm^2)
S is the mass stopping power and is a function of energy (MeV·cm^2·g^{-1})
E is the energy of the incident projectile
$\int_{E_f}^{E_i}$ is the integral from initial, E$_o$, to final energy, E$_f$, of the projectile
A is the activity of nuclei i being produced (Bq)

The production rate of an isotope is directly related to the area under the reaction cross-section curve that spans over a given entry and exit energies (Rowshanfarzad et al., 2006). This is due to the energy loss of the projectile as it traverses through the target, defined by the stopping power. The reaction cross section acts as a function of projectile energy, changing throughout each segment of the target that the projectile traverses. Equation 1 takes this into account by integrating the reaction cross section and stopping power, both as a function of projectile energy, for a given projectile traversing a given target material to acquire the effective area under the reaction probability curve. The thickness of the target material dictates the exit energy, E_0, of the projectile and ultimately the length of the reaction probability curve.

Other important parameters that directly affect the production rate include the total number of incoming particles (beam current) and the saturation factor (SF). The production rate is directly proportional to the beam current. Large beam currents can cause substantial overheating capable of melting the target; therefore, careful thermal and mechanical stress analysis of the target must be carried out to safely produce a radionuclide. Overheating concerns can be addressed through different methods such as altering the irradiation time and beam current or adjusting the incident angle by which the beam strikes the target (Agency, 2009b).

The saturation factor, SF, is given by $(1 - e^{-\lambda t})$ and is the measure of the practical production limits of a given radionuclide. This is typically determined by the half-life of the isotope where irradiation times rarely exceed more than 3 half-lives, ~90% saturation, of the isotope. When the saturation activity of a radionuclide is

21

achieved during irradiation, the number of nuclei of that radionuclide being produced is equal to the number undergoing radioactive decay. It takes approximately 8 half-lives to reach the saturation activity which can result in significant irradiation times when considering longer lived radionuclides. As a result, considerations must be given for the expected yield of the longer lived radionuclides relative to the length of bombardment (Agency, 2009b).

In this study, Equation 1 was used to calculate the theoretical production yields for ^{62}Zn and contaminants (Table 5) for proton entry energies between 18 and 30 MeV. Given that the area under the reaction cross-section curve is dictated by both the entry and exit energy of the proton beam relative to the thickness of the copper target, the theoretical production yields were modeled for varying target thicknesses as well. The target thicknesses investigated were between 0.1 and 1.5 mm, each over the same proton entry energy range between 18 and 30 MeV.

The accuracy of Equation 1 was quantified by using irradiation parameters listed in previous studies to calculate theoretical production yields for ^{62}Zn. The theoretical production yields were compared against measured ^{62}Zn production yields reported in the respective studies. The results of this analysis is reported in the Results section and subsequently used to apply a correction factor to the theoretical yield. Table 6 shows the irradiation parameters used in each study. Reaction cross-section data was taken from a Java-based Nuclear Information Software (JANIS) developed by the Nuclear Energy Agency (Soppera et al., 2014).

Table 6. The values for proton entry energy, target diameter, target thickness, number of discs used, beam current, and irradiation time used in previous papers.

Reference	Projectile Energy	Target Mass	Target Thickness	# of Cu Discs	Beam Current	Irradiation Time
	(MeV)	(g)	(mm)	(#)	(µA)	(h)
Zweit et al., 1992	33.6	4.48	1.6	3	25	1
Robinson et al., 1980	22	3.45	0.4	2	30	1
Fukumura, 2006	29.7	2.06	0.9	1	10	1
Bormons et al., 1992	27	1.70	0.5	1	40	1
Lacy et al., 1998	33	-	1.62	1	37.5	0.75

2.2.5   Estimating Radiation Exposure

The production yield of ^{62}Zn is directly affected by the external radiological hazard presented by the short-lived contaminants produced during irradiation. Each short-lived contaminant contributes in varying degrees of intensity to the gamma-ray radiation field around the target. To be in compliance with 10CFR20.1301, the dose equivalent rate to an unrestricted area from an external radiation source must be less than 20 µSv·hr^{-1} (2 mRem·hr^{-1}). This regulatory limit requires a cooling period after EOB where the target must sit to allow for the decay of the short-lived contaminants that compose the largest component of the external radiological hazard around the target (Robinson Jr et al., 1980; Zweit et al., 1992). The larger quantity of short-lived contaminants that are produced, the longer the target must sit to allow for their decay. As a result, the short-lived contaminants directly affect ^{62}Zn's production yield as it can go through as much as one to two half-lives during the cooling period. Estimating the radiation exposure levels around the target provides an estimate of the length of the

23

necessary cooling period after EOB. Thus, to effectively optimize the production yield of ^{62}Zn, the radiation exposure levels around the target were estimated for proton entry energies between 18 and 30 MeV.

The irradiated target was modeled as a gamma-ray emitting point source contained in a 5 cm thick lead pig (Figure 5). The product and contaminants that were modeled are listed in Table 7. Each of these radionuclides j have an activity that emits N gamma-rays with a respective emission rate Y_i for each gamma-ray i. To calculate the absorbed dose, it was assumed that electronic equilibrium existed in tissue at a distance 1.0 m from the target. Given that gamma-rays are the only penetrating radiation that contribute to the radiation exposure around the target, a quality factor of 1 was assigned. Lastly, attenuation by air was considered negligible but buildup of the dose equivalent rate due to secondary radiations generated by photon interactions with the lead shielding was included into the calculations. Given these assumptions, the dose equivalent rate at a distance of 1.0 m from the irradiated was calculated with Equation 2 (Turner, 2008).

Figure 5. Lead pig used to unload the target disk. The walls of the lead pig are 5.0 cm thick.

$$\dot{H}_T = \sum_{j=1}^{7} \sum_{i=1}^{N} \frac{A_j Y_i E_i k}{4\pi r^2} \left(\frac{\mu_{en}}{\rho}\right)_{i,T} B_i e^{-\mu_i x} e^{-\lambda_j t} Q \tag{2}$$

where

$\dot{H}_T$ is the total dose equivalent rate in air (μSv·hr^{-1})
A_i is the activity of radionuclide j (s^{-1})
E_i is the energy for a given photon i emitted by radionuclide j (MeV)
$\frac{\mu_{en}}{\rho}$ is the mass energy-absorption coefficient of tissue for photon i (cm^2·g^{-1})
μ_i is the linear attenuation coefficient in lead for photon i (cm^{-1})
x is the thickness of the lead shielded pig (cm)
B_i is the buildup factor given $\mu_i x$, the mean free path in lead for photon i
r is the distance from the irradiated target (cm)
k   is a conversion factor of 0.577 to go from MeV·g^{-1}·s^{-1} to μSv·hr^{-1}
λ is the decay constant for radionuclide j (hr^{-1})
t   is the cooling period after EOB (hr)
Q   is the radiation quality factor

Modeling the irradiated target as a point source allowed for the dose equivalent rate to be calculated for each radionuclide and subsequently summed to acquire the total dose equivalent rate. The cooling period after EOB was determined with an iterative method that increased the cooling period in increments of 1 hour until the total dose equivalent rate around the target was below the federal limit. If the total dose equivalent rate was greater than the 20 μSv·hr^{-1}, an additional hour was added and the activity for each radionuclide was decay corrected using the new cooling period. This process was repeated for proton entry energies of 18 to 30 MeV.

The energy and yield of each photon emitted by the radionuclides in Table 7 were obtained from the National Nuclear Data Center's (NNDC) Nuclear structure and Decay data (NuDat) database. The activities for each radionuclide were calculated with

the use of Equation 1. The linear attenuation coefficients for lead and mass energy-absorption coefficients for tissue were acquired from the X-Ray and Gamma-Ray Data section of the National Institute of Standards and Technologies (NIST) website. The buildup factors for lead were obtained from the Health Physics and Radiological Health Handbook (Shleien and Terpilak, 1992).

Table 7. The product ^{62}Zn and relevant contaminants present in an irradiated target after bombardment.

Type	Radionuclides in Irradiated Target
Product	zinc-62
Contaminants	zinc-63
	zinc-61
	copper-61
	cobalt-58
	zinc-65
	copper-64

2.2.6   Targetry

The target consists of a solid high purity natural copper disc. Copper can be purchased at low cost as a single high purity foil and requires little pre-fabrication prior to irradiation depending on the form. Isotopic enrichment is not required due to the high isotopic abundance of copper-63. Due to this, recycling of the copper target for re-use in future irradiations is not a concern.

Previous experiments commonly cite the use of solid copper discs (Bormans et al., 1992; Fukumura, 2006; Haynes et al., 2000; Robinson Jr et al., 1980; Zweit et al.,

1992). Other types of targets are available, such as the use of electroplating copper onto a backing material (Fujibayashi, 1989). The copper discs can be irradiated as a stack of thin discs (Robinson Jr et al., 1980; Zweit et al., 1992) or as a single thick disc (Bormans et al., 1992; Fukumura, 2006; Haynes et al., 2000). The target has a backing material that typically possesses several desirable qualities such as a high thermal conductivity, low chemical reactivity, low activation cross sections, easy to machine, and high mechanical strength (Agency, 2009b). The backing material should be capable of transferring heat generated in the target to a heat sink while maintaining its integrity. For this reason, the most common material used as a backing material is aluminum (Agency, 2009b). Aluminum is advantageous due to its high thermal conductivity, activation products are short-lived and produced in low abundance, is chemically inert and very malleable (Agency, 2009a).

The most common method of heat dissipation is water cooling against the back of the target. In previous experiments, the water cooling has been listed at 4 L/min against the back of the target (Zweit et al., 1992) or designed such that the back of the target is maintained at 20 °C (Fukumura, 2006). Helium gas cooling directly against the front of the target, maintaining a temperature of -30 ºC, has been utilized previously as well.

Target thickness, target diameter, and number of disks used in previous papers are listed in Table 6. Important aspects of targetry used in this study involve the use of SRIM nuclear code (Ziegler, 2004) to create a simple model that was able to determine the rate of energy deposition for a proton traversing a copper target. Figure 6 shows this

27

model, which consists of a curve representing the proton range in copper for energies

between 1 and 50 MeV. Figure 6 provides the necessary data to calculate the exit energy

of a proton with a given entry energy and target thickness. Knowing the entry and exit

energy for a given target, the energy deposition every 30 microns was calculated to

provide an accurate assessment of the energy loss of the proton as it traversed through

the target. This was incorporated into calculations using Equation 1. More detailed

information about cyclotron targetry for solid targets, target preparation, and target

irradiation practices and procedures can be found in Technical Report Series No. 465

Cyclotron Produced Radionuclides: Principle and Practice published by the IAEA.
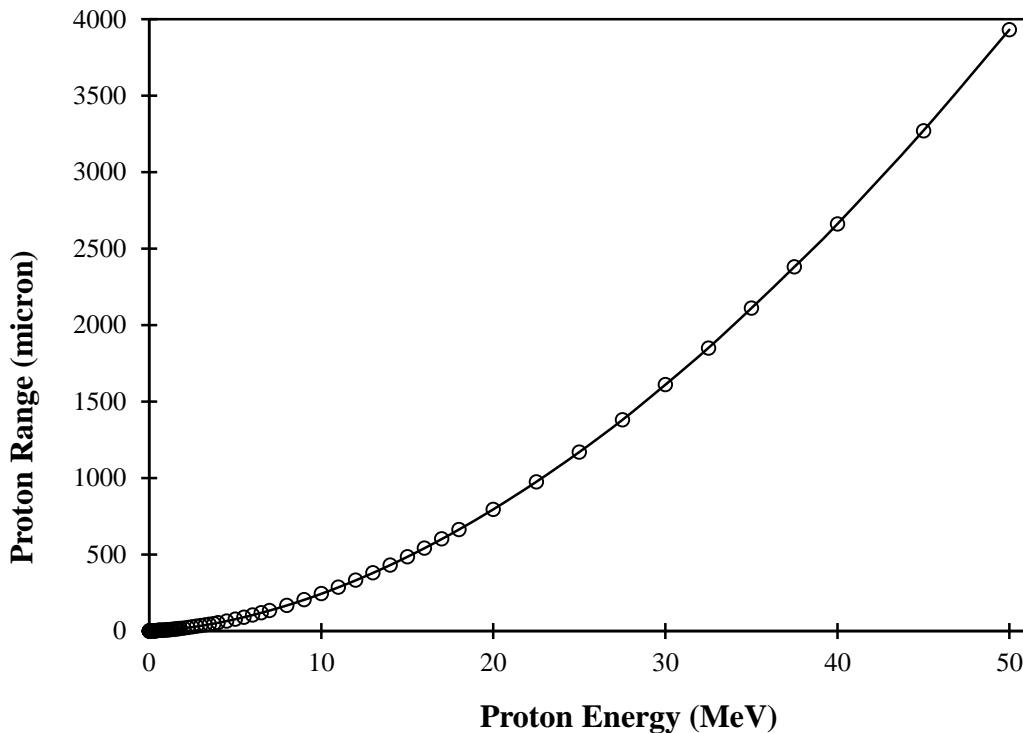
Figure 6. The proton range in copper for proton energies between 1 and 50 MeV. Data
was taken from SRIM nuclear code (Ziegler, 2004).

2.3   Target Processing

2.3.1   Alternative Target Processing Method

Previous methods for target processing utilize concentrated hot nitric acid (an oxidizer) to quickly dissolve the target down to a copper(II) nitrate ($Cu(NO_3)_2$) solution. This solution was heated to decompose the copper(II) nitrate to copper(II) oxide (CuO), which precipitated out of the solution. When mixed with concentrated hydrochloric acid, copper(II) oxide undergoes a displacement reaction that results in the formation of the coordinate complex, copper(II) chloride ($CuCl_2$). Chemical separation of zinc and copper is based off the difference between their chloride complex formations (Fujibayashi, 1989). This process produces a large volume of corrosive fumes due to the use concentrated hydrochloric and nitric acid.

In this study, an alternative target dissolution method was developed that sought to eliminate the volume of corrosive fumes generated during the target processing phase. This alternative dissolution method involved the use of 30% hydrogen peroxide (H_2O_2) and 2 M hydrochloric acid to dissolve a copper foil representative of an irradiated copper target. The copper foil was placed in a solution of dilute HCl and hydrogen peroxide was added. The hydrogen peroxide will act as an oxidizer that dissolves the copper target, freeing copper(II) ions into the solution. The decomposition of hydrogen peroxide is an exothermic reaction and will release significant amounts of heat into the solution. Thus, the temperature of the solution will be monitored with a glass thermometer. Chloride ions in the solution from the HCl will form coordinate complexes with the copper(II)

29

ions, forming the desired copper(II) chloride complex. This chemical reaction is depicted in Equation 3.

$$H_2O_{2(aq)} + Cu_{(s)} + 2\,H^+_{(aq)} \rightarrow Cu^{2+}_{(aq)} + 2\,H_2O_{(l)}$$

$$Cu^{2+}_{(aq)} + 4\,Cl^-_{(aq)} \rightarrow [CuCl_4]^{2-}_{(aq)} \tag{3}$$
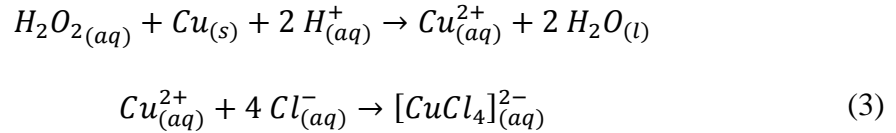
Following the complete dissolution of a copper foil with the alternative dissolution method, an alternative target processing procedure was developed. This involved the use of copper foils that represented a small copper target with a thickness of 1.0 mm, radius of 6.0 mm, and mass of 1.0 g. The copper was purchased from Sigma Aldrich in the form of a 1.0 mm thick sheet of high purity natural copper. The copper foils cut from this sheet were smaller than the typical copper target of 1.75 to 4.50 g used in previous references (Table 6).

2.4   Chemical Processing

2.4.1   Ion Exchange Chromatography

The accepted technique for separating ^{62}Zn from the solution obtained at the end of the target processing phase is Ion Exchange Chromatography (IEC) (Bormans et al., 1992; Fukumura, 2006; Robinson Jr et al., 1980; Zweit et al., 1992). This technique is preferred due to its extremely high separation efficiency with divalent transition metals. Commonly, the AG-1 (Fukumura, 2006; Zweit et al., 1992) or Dowex-1 (Bormans et al., 1992; Robinson Jr et al., 1980) anion exchange resin in the chloride form is used as the

stationary media within the column. The resin consists of an insoluble matrix that contains bonded functional groups referred to as fixed ions that can be either cationic or anionic (Haddad, 1994). The AG-1 and Dowex-1 resin are both strongly basic with cationic quaternary amino groups, N^+R_4, as the fixed ion. The chloride form indicates that the counter-ion is a Cl^- atom. When passing a solution through the column, ion exchange occurs between the solution in the mobile phase (eluent) and the counter-ion in the stationary phase (resin). The counter-ion can only exchange with another ion in the solution that has a similar charge and a higher affinity for the resin.

The anionic chloride complex that ^{62}Zn and the other contaminants form can exchange with the chloride counter-ions and subsequently be captured on the AG-1 and Dowex-1 resins. The affinity of each type of chloride complex to bind to the resin over the chloride counter-ion is determined by the divalent transition metal at the center of the chloride complex. The large difference in anion exchange behavior between each divalent transition metal is likely due to the large difference in their complexing properties as a function of atomic number (Kraus, 1953). It was observed by Kraus,1953 that the order of complexing strength is directly proportional to the solubility of each metal in hydrochloric acid and how readily they form chloride complexes (Kraus, 1953). For transition metals such as zinc, which dissolve readily in hydrochloric acid, stronger chloride complexes are formed that have a higher affinity to exchange with the chloride counter-ion and bind to the resin than the weaker chloride complexes formed by the contaminants. Figure 7 shows that zinc has an adsorption maximum with a strong anion exchange resin in a 2 M HCl solution while the transition metal contaminants have

31

significantly less adsorption affinities to the resin at the same concentration. It is this

difference in adsorption affinities between zinc and the contaminants that allows the

contaminants to be separated by direct elution with 2 M HCl while zinc isotopes remain

captured in the resin. Additional detailed information behind the use of ion exchanged

chromatography in the chemical processing procedure can be found in Zweit, et al., 1992

and Fukumura, 2006.
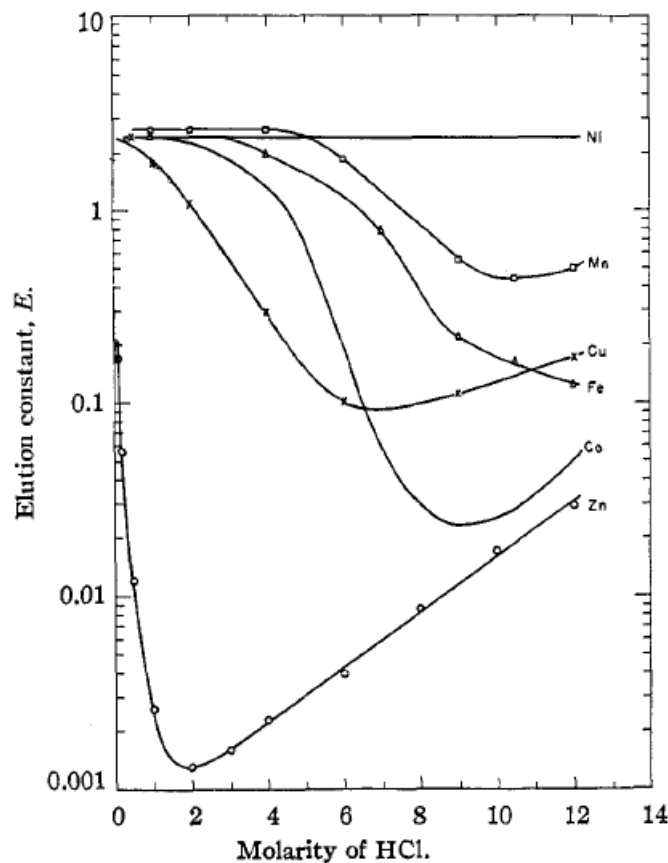
Figure 7. Profile of elution constants taken from Kraus,1953 that depict the adsorption properties of divalent transition metals in a HCl solution with strong anion exchange resin (Kraus, 1953). The elution constant is obtained with $E = dA/V$, where d is the distance (cm) that an adsorption maximum travels when passing an amount of V (cm^3) eluent through a column with cross-sectional area A (cm^2).

2.5   The ^{62}Zn/^{62}Cu Generator Column

The procedure for loading the generator column has been established in previous studies (Haynes et al., 2000; Robinson Jr et al., 1980; Zweit et al., 1992). The generator column itself is composed of a commercially available borosilicate glass column with volumes ranging between 0.75 and 3.85 ml. The generator column is housed inside of a cylindrical lead shield appropriately thick to reduce radiation exposure levels around the generator to below federally regulated limits dictated by 10CFR20.1301. The lead shielding contains input and output ports connected to the top and bottom of the glass column, respectively. These ports allow for loading of ^{62}Zn and elution of ^{62}Cu from the generator column. The generator column is loaded with AG1 anion-exchange resin (Cl$^-$) and is pre-equilibrated with 0.3 M HCl/40% ethanol for maximum elution yield of ^{62}Cu (Zweit et al., 1992). Different ligand structures, different concentrations, and their effect on ^{62}Cu elution yield and ^{62}Zn leakage have been analyzed by Fujibayashi, 1989 (Fujibayashi, 1989).

2.6   Automating Generator Production

2.6.1   Necessary Hardware

Two single channel OEM model NE-500 syringe pumps were purchased from New Era Pump Systems Inc (Figure 8). The OEM version of the NE-500 model comes with the pump internals attached to a chassis that is mountable. The dimensions of the chassis are 24.13 x 10.16 x 10.5 cm^3. This model type holds a single syringe that is capable of infusion and withdrawal pumping of syringe volumes up to 60 cc full or 140

cc partially filled. Pumping rates with this model can range from as low as 0.73 $\mu l \cdot hr^{-1}$ with a 1 cc syringe to 2120 $ml \cdot hr^{-1}$ with a 60 cc syringe. Detailed information involving syringe types from different manufacturers, their offered syringe volumes, those syringe inner diameters, minimum rate and maximum rate is contained in Table 8. The NE-500 communicates through an RS-232 connection, labeled "To Computer" on the instrument, which connects directly to an RS-232 port on a computer. The NE-500 is also capable of operating in a network with other instruments through a secondary RS-232 connection labeled "To Network". This instrument network can support up to 100 instruments and is not limited solely to the NE-500.
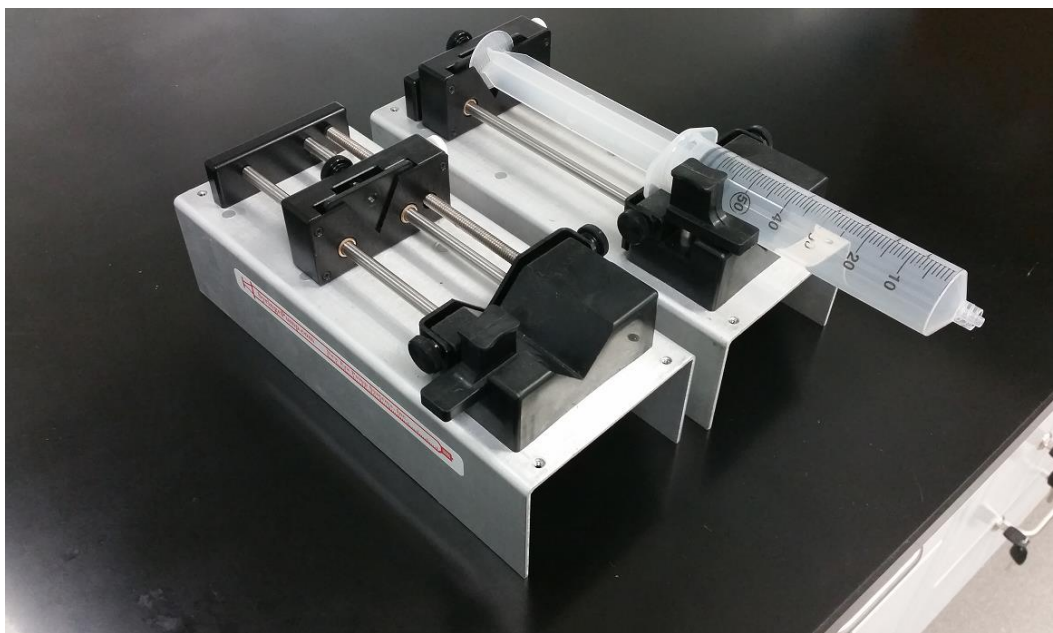
Figure 8. Two single channel OEM model NE-500 syringe pumps.

One syringe heater model HEATER-KIT-1LG was purchased from New Era Pump Systems Inc (Figure 9). The electronics of the HEATER-KIT-1LG are contained

in a case that allows direct manipulation of the instrument through external controls. More importantly, the instrument also contains the same RS-232 connections as the NE-500. The case was not purchased as an OEM version and has dimensions of 11.75 x 6.35 x 3.81 cm^3. The heating element of the instrument is a thermocouple contained in a heating pad with the dimensions 8.8 x 7.5 cm^2. The heating pad is intended to be wrapped around a syringe or item of similar shape. The maximum temperature of the heating pad is 185 °C.
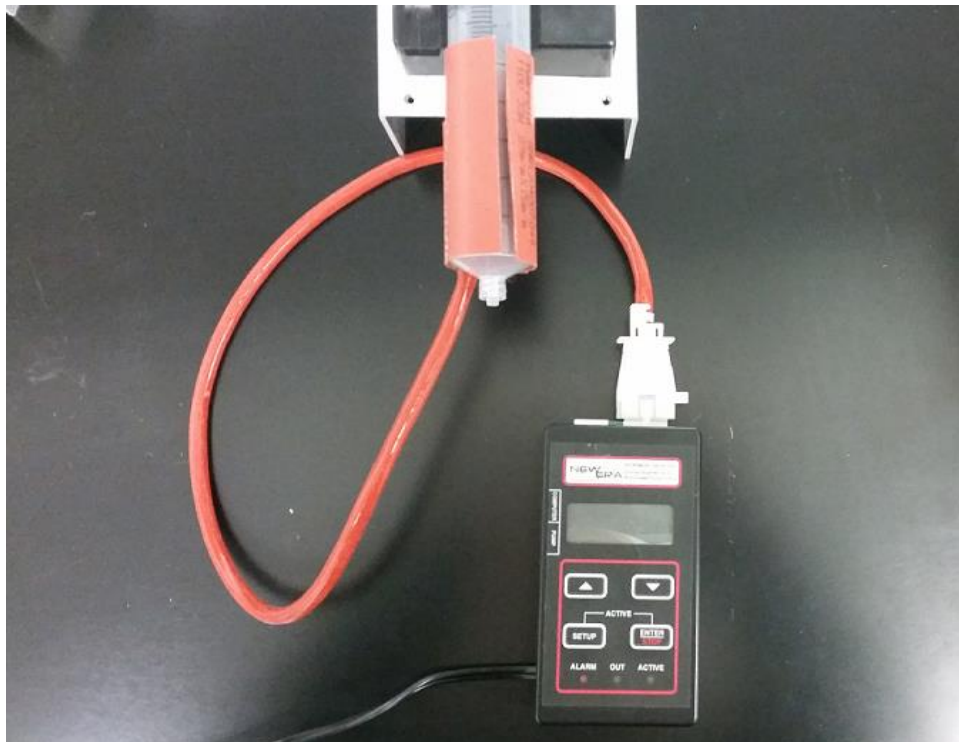
Figure 9. A single syringe heater model HEATER-KIT-1LG.

Table 8. A list of syringe diameter and rate limits for the NE-500 pump using syringes from different manufacturers. This data was taken from the NE-500 syringe pump user manual.

Syringe Manufacturer	Syringe Volume (mL)	Inside Diameter (mm)	Maximum Rate (mL·hr⁻¹)	Maximum Rate (mL·min⁻¹)	Minimum Rate (µL·hr⁻¹)
B-D	1	4.70	53.07	0.88	0.73
	3	8.59	177.10	2.95	2.43
	5	11.99	345.50	5.76	4.75
	10	14.43	500.40	8.34	6.88
	20	19.05	872.20	14.53	11.99
	30	21.59	1120.00	18.67	15.40
	60	26.59	1699.00	28.32	23.35
HSW Norm-Ject	1	4.69	52.86	0.88	0.73
	3	9.65	223.80	3.73	3.08
	5	12.45	372.50	6.21	5.12
	10	15.90	607.60	10.12	8.35
	20	20.05	966.20	16.10	13.28
	30	22.90	1260.00	21.00	17.32
	50	29.20	2049.00	34.15	28.16
Monoject	1	5.74	79.18	1.32	1.09
	3	8.94	192.10	3.20	2.64
	6	12.70	387.60	6.46	5.33
	12	15.72	593.90	9.90	8.16
	20	20.12	972.90	16.21	13.37
	35	23.52	1329.00	22.15	18.27
	60	26.64	1705.00	28.42	23.44
	140	38.00	3470.00	57.84	47.69
Terumo	1	4.70	53.09	0.88	0.73
	3	8.95	192.50	3.21	2.65
	5	13.00	406.10	6.77	5.58
	10	15.80	600.00	10.00	8.24
	20	20.15	975.80	16.26	13.41
	30	23.10	1282.00	21.37	17.63
	60	29.70	2120.00	35.33	29.13

One USB Digital I/O Device OEM model USB-6501 was purchased from National Instruments (Figure 10). The OEM version of the USB-6501 is mountable with the dimensions 5.74 x 6.73 cm^2. The instrument has 24 digital I/O lines capable of both sending output logic pulses of 0 V (off) or 5 V (on) and receiving data in the form of logic pulses. The 24 channels are broken up into three different ports of 0, 1, and 2 with 8 channels each. The instrument has a generic 34-pin connection that can be interfaced with any commercially available 34-pin IDC female connector where each pin correspond to different I/O channels and ground connections. The pin assignments for the USB-6501 are shown in Table 9. The USB-6501 communicates with a computer through a USB connection. A detailed summary of all of the hardware purchased, their necessary accessories, and dimensions is contained in Table 10.
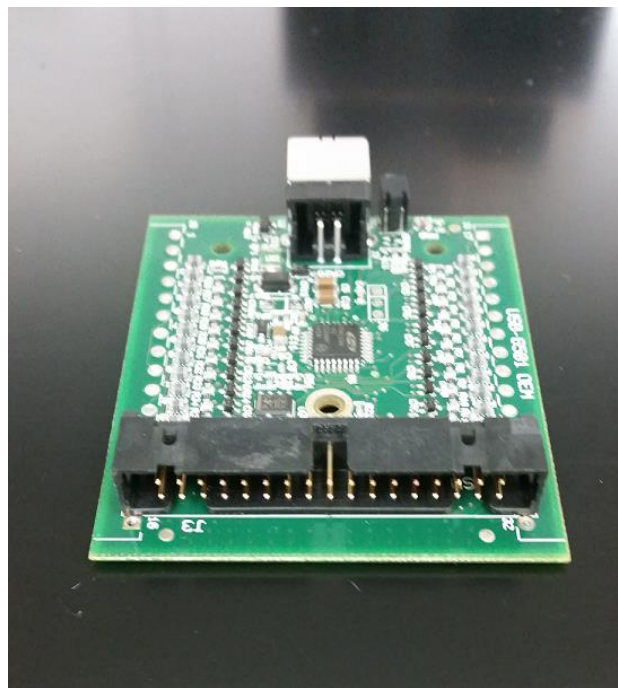
Figure 10. A single USB Digital I/O Device OEM model USB-6501 with 34 pins.

Table 9. The pin assignments for Ports 0-2 on the USB-6501 taken from the OEM User Guide.

Signal	Pin	Connector	Pin	Signal
P1.0	1		2	GND
P1.1	3		4	P2.0
P1.2	5		6	GND
P1.3	7		8	P2.1
P1.4	9		10	GND
P1.5	11		12	P2.2
P1.6	13		14	GND
P1.7	15		16	P2.3
P0.0	17		18	GND
P0.1	19		20	P2.4
P0.2	21		22	GND
P0.3	23		24	P2.5
P0.4	25		26	GND
P0.5	27		28	P2.6
P0.6	29		30	GND
P0.7	31		32	P2.7
+5V	33		34	+5V

Connector diagram labels: Pin 1, Pin 2, Pin 33, Pin 34

Table 10. A summarized list of the hardware components purchased, their company, relevant accessories, interface, and dimensions.

	Syringe Pump (NE-500)	Syringe Heater (HEATER-KIT-1LG)	Digital I/O (USB-6501)
Hardware	Syringe Pump (NE-500)	Syringe Heater (HEATER-KIT-1LG)	Digital I/O (USB-6501)
Company	New Era Pump Systems Inc	New Era Pump Systems Inc	National Instruments
Accessory	CBL-PUMP	CBL-PUMP	34 pin connector
Interface	RS-232	RS-232	USB
Dimensions	$24.13 \times 10.16 \times 10.5$ cm^3 (L x W x H)	54 cm long cord 8.8×7.5 cm^2 (pad) (L x W) $11.75 \times 6.35 \times 3.81$ cm^3 (case) (L x W x H)	5.74×6.73 cm^2 (L x W)

2.6.2   Necessary Software

The RS-232 connection on the NE-500 is commonly referred to as a serial port

and works by sending data one bit at a time. To successfully communicate with the NE-

500, a software that was capable of interpreting serial communication was utilized. The

software LabVIEW, developed by National Instruments, was particularly well suited for

this task. LabVIEW is short for Laboratory Virtual Instrument Engineering Workbench

and is a visual programming software put out by National Instruments for use as a

system-design platform. LabVIEW consists of two windows: the front panel and block

diagram. The front panel is considered the user interface (UI) where controls, inputs, and

outputs are connected to code or programming in the block diagram. The front panel

represents a completely customizable UI that can be geared toward virtually any

application. LabVIEW uses its Virtual Instrument Software Architecture (VISA) as a

standard for configuring and programming instrument systems that communicate over

serial or USB connections. The VISA interface software comes separately from

LabVIEW and must be downloaded and installed manually from National Instruments

website.

The NE-500 was controlled with programming developed in LabVIEW.

Communications to and from the NE-500 occur through a RS-232 or serial port

connection with a computer. LabVIEW must configure the serial port with the same

baud rate and data frame as the NE-500 to successfully communicate with the

instrument. The data frame information for the NE-500 is listed in Table 11.

Table 11. The RS-232 data frame used by the NE-500 Syringe Pump to communicate through a serial connection.

RS-232 Data Frame	
Baud Rate:	19200
Frame:	10 Bit Data Frame (8N1)
Start Bit:	1
Data Bit:	8
Stop Bit:	1
Parity	None

The NE-500 is controlled by sending commands to the instrument with LabVIEW. When commands are sent, the NE-500 processes it and sends a response back to the serial port. It is important to note that once a command has been sent to the NE-500, it will not accept any further communications until the command has been processed. Commands and responses with the NE-500 consist of characters that are a combination of ASCII codes and numeric data. The numeric data is classified as a floating point number with 4 digits and 1 decimal point. Commands sent to the NE-500 should have a carriage return, 0x0D in ASCII, at the end. Space characters that are placed within the command will be ignored when processed by the pump and can be considered optional when giving inputs.

An instrument network can technically support 100 instruments with addresses from 00 to 99. When the NE-500 is used in a network, each instrument must be assigned an address. The default address for each instrument is 00 and must be set with a direct connection to the port labeled "To Computer" prior to being connected to the network. When placing an instrument into a network, the first instrument must have a connection from the port labeled "To Computer" to the RS-232 port on the computer. Every

instrument after the primary instrument must have a connection from the port labeled "To Network" on the prior instrument to the port labeled "To Computer" on the subsequent instrument. When issuing commands to an instrument in a network, the address number of the desired pump must precede the command.

Table 12 provides simple examples illustrating the syntax of how a command should be sent to the NE-500. Table 13 contains a list of commands taken by the NE-500, their purpose, and the NE-500's query response for each command. Table 12 can be used as a supplement to provide examples of syntax for the various commands in Table 13. More information about the NE-500 syringe pump can be found in the NE-500 OEM Syringe Pump User Manual.

Table 12. A list of examples illustrating the appropriate syntax for a set of common commands and a brief explanation behind what each command does.

Command	Syntax	Explanation
ADR	ADR10x0D	Assign Address 1 to pump
DIA	ADRDIA200x0D	Assign inner diameter of syringe to 20 mm. ID > 10 sets units to mL
VOL	ADRVOL50x0D	Assign 5 mL to be dispensed
RAT	ADRRAT30MM0x0D	Assign a pumping rate of 30 mL/min
DIR	ADRDIRINF0x0D	Assign a pump direction: Infuse
RUN	ADRRUN0x0D	Set pump to run. Infuse 5 mL automatically.

The HEATER-KIT-1LG operates under the same technical and programmable principles as the NE-500. It has an RS-232 port that allows LabVIEW to control it through its VISA interface software. The HEATER-KIT-1LG can operate in the same instrument network as the NE-500 with its own designated address. Additionally, this

instrument uses the same data frame (Table 11) and the same command syntax (Table

12) as the NE-500. However, unlike the NE-500, data changes are not automatically

stored in its non-volatile memory unless a save command is given to the syringe heater.

Table 14 contains a detailed list of commands taken by the HEATER-KIT-1LG, their

purpose, and the HEATER-KIT-1LG's query response for each command. More

information about the instrument can be found in the Syringe Heater User Manual.

Table 13. A list of commands, their numeric argument, their purpose, and the
instruments response when queried with each command for the NE-500, taken from the
NE-500 user manual.

Command	Numeric Argument	Purpose	Instrument Response
DIA	<float>	Syringe Inner Diameter. (0.1 to 10 mm - UL) (10.01 to 50 mm - ML)	<float><units>
RAT	[<float>< units>]	Pumping Rate with units (UM,UH,MM,MH)	<float><units>
VOL	[<float> | <units>]	Volume to be dispensed Manually set volume units (ML,UL)	<float><units>
DIR	[INF | WDR]	Pumping Direction	[INF | WDR]
RUN	-	Starts the pumping program	-
STP	-	Stops the pumping program	-
DIS	-	Query volume dispensed	I<float>W<float><units>
CLD	[INF | WDR]	Clear volume dispensed	-
SAF	<n>	Safe communications mode (n = 0 to 255)	<n>
AL	[<on-off>]	Alarm mode	[<on-off>]
PF	[<on-off>]	Power failure mode	[<on-off>]
BP	[<on-off>]	Key and notification beep mode	[<on-off>]
VER	-	Query firmware version	NE50<n>V<n>.<nn>
ADR	<n>	Network Address	<n>
RESET	-	Clears memory and resets all values	-

Table 14. A list of commands, their numeric argument, their purpose, and the instruments response when queried with each command for the HEATER-KIT-1LG, taken from the Syringe Heater user manual.

Command	Numeric Argument	Purpose	Instrument Response
RUN	-	Enter active mode Maintain heating temp	-
STP	-	Exit Active Mode	-
TMP	-	Query heating pad temp	<n>
SET	<n>	Set heating setpoint	<n>
FTS	<n>	Set fine tune slow down degree setting	<n>
FTH	<n>	Set fine tune temp hold percentage	<n>
SAV	-	Save all new settings in non-volatile memory	-
UNT	[C | F]	Set temp units	[C | F]
PF	[<on-off>]	Alarm mode	[<on-off>]
CAL	[L | H [<n>]]	Heating pad calibration	-
PAD	<n>	Calibration setting 1 - Default 0 - Calibrated	<n>
ADR	<n>	Set network address	<n>
VER	<n>	Query firmware version	NE8<nn>V<n>.<nn>
RESET	-	Clears memory and resets all values	-

As with the serial connection, the same principle applies to a USB connection. The USB-6501, with a USB connection, requires the VISA interface driver to interact with LabVIEW as well. However, because the USB-6501 is a data acquisition (DAQ) device, it also requires additional software drivers from National Instruments to successfully interface with LabVIEW. These software drivers are NI-DAQmx and NI-DAQmx Base and are found on the National Instruments website. NI-DAQmx allows LabVIEW to communicate with the USB-6501 and NI-DAQmx Base provides

43

specialized functionality for controlling the USB-6501. The NI-DAQmx Base allows for

the use of an automated function known as the DAQ Assistant. The DAQ Assistant will

take inputs designated by the user and apply them to automatically generated

programming that will change the trigger states of the different I/O channels as

indicated. In this case, the trigger state represents the on/off state of each channel. It is

worth noting that the software drivers from National Instruments are free and

automatically update through LabVIEW's driver management software when new driver

updates are published. A summary of the necessary hardware components and the

software drivers required to use them in LabVIEW is contained in Table 15.

Table 15. Hardware components and their required software.

Hardware Component	National Instrument Software Drivers		
	NI-VISA	NI-DAQmx	NI-DAQmx Base
NE-500	✓	✗	✗
HEATER-KIT-1LG	✓	✗	✗
USB-6501	✓	✓	✓

3. RESULTS AND DISCUSSION

3.1 Results

3.1.1 Optimal Irradiation Parameters

Between proton entry energies of 18 and 30 MeV, the only reaction utilized to produce ^{62}Zn is ^{63}Cu(p,2n). However, both ^{63}Cu and ^{65}Cu are utilized in the production of the contaminants listed in Table 5. Theoretical yields at EOB for ^{62}Zn were calculated for target thicknesses of 0.1, 0.5, 1.0, and 1.5 mm. These values, shown in Figure 11, illustrate that the yield of ^{62}Zn increases both as a function of proton entry energy and target thickness up to a maximum.
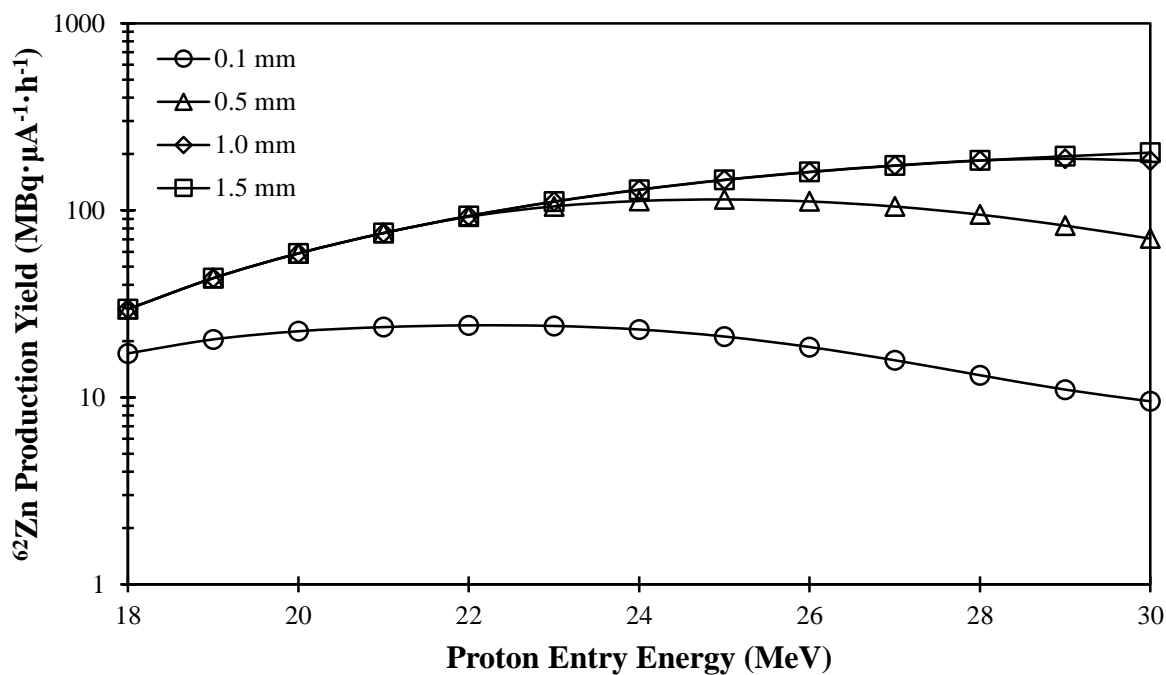
Figure 11. Theoretical ^{62}Zn production yield at EOB with target thicknesses between 0.1 and 1.5 mm for proton entry energies between 18 and 30 MeV.

The ^{62}Zn yield increases with target thickness up to 1.0 mm with diminishing returns on

any additional increase in thickness 1.0 mm. Thus, it was observed that the ^{62}Zn yield at

EOB for a 1.0 mm thick target was essentially identical to that of a 1.5 mm thick target

over the same proton energy range. The results from Figure 11 indicated that the optimal

target thickness for the routine production of ^{62}Zn was 1.0 mm.

Utilizing a target thickness of 1.0 mm, the dose equivalent rate in tissue at a

distance of 1.0 m was calculated for each radionuclide (Table 7) and summed for the

whole target. The cooling period after EOB was calculated based upon the regulatory

dose limit set by 10CFR20.1301. The EOB dose equivalent rates for each radionuclide

and for the target are shown in Table 16.

Table 16. The EOB dose equivalent rate at 1.0 m for each radionuclide and the total dose equivalent rate for the target.

Proton Entry Energy	Radionuclide Dose Rates							Target Dose Rate
	Zn-62	Zn-63	Zn-61	Cu-61	Co-58	Zn-65	Cu-64	
(MeV)				(μSv·hr^{-1})				(μSv·hr^{-1})
18	0.0	94	0	0	0	1	0	95
19	0.1	97	0	0	0	1	0	98
20	0.1	99	0	0	0	1	0	100
21	0.1	101	0	0	0	1	1	103
22	0.1	103	0	0	0	1	1	105
23	0.1	105	0	0	0	1	1	107
24	0.2	102	0	0.1	0	1	1	105
25	0.2	90	0	0.3	0	1	1	92
26	0.2	75	0	1	0	1	1	77
27	0.2	58	0	1	0.0000	0	2	61
28	0.2	41	0	3	0.0001	0	2	46
29	0.2	32	0.1	4	0.0003	0	2	38
30	0.2	27	0.3	6	0.0006	0	2	35

^{63}Zn ($T_{1/2}$ = 38.47 min) dominates between 75 and 99% of the total dose equivalent rate from the target over proton entry energies between 18 and 30 MeV. At proton entry energies of 29 and 30 MeV, ^{61}Cu ($T_{1/2}$ = 3.33 h) dominates 10 and 17% of the total dose equivalent rate, respectively. The other contaminants contribute to 5% or less of the total dose equivalent rate around the target.

The cooling period after EOB is 2 hours from 18 to 27 MeV and 1 hour from 28 to 30 MeV. Using the cooling period for each proton entry energy, the production yield of each radionuclide was decay corrected. The ^{62}Zn production yields for proton entry energies between 18 and 30 MeV, decay corrected with their respective cooling periods, are shown in Table 17.

Table 17. The production yield for each radionuclide, decay corrected with their respective cooling period at each proton entry energy.

Proton Entry Energy	Cooling Period	Radionuclide Production Yields						
		Zn-62	Zn-63	Zn-61	Cu-61	Co-58	Zn-65	Cu-64
(MeV)	(hr)	$(MBq \cdot \mu A^{-1} \cdot h^{-1})$						
18	2	25	603	0	0	0.000	1.40	85
19	2	37	619	0	0	0.000	1.43	123
20	2	51	634	0	0	0.000	1.46	169
21	2	65	648	0	0	0.000	1.48	222
22	2	80	662	0	0	0.000	1.50	283
23	2	96	674	0	1	0.000	1.53	351
24	2	111	656	0	4	0.000	1.43	423
25	2	125	575	0	11	0.000	1.19	497
26	2	138	478	0	27	0.000	0.88	572
27	2	149	369	0	56	0.000	0.59	646
28	1	171	780	0	125	0.003	0.43	756
29	1	175	596	0	204	0.009	0.34	813
30	1	171	502	0	306	0.020	0.30	850

A maximum ^{62}Zn yield of 175 MBq·µA^{-1}·h^{-1} was observed at a proton entry energy of

29 MeV. The ^{65}Zn/^{62}Zn ratio is approximately 0.2% at 29 MeV proton entry energies.

The calculated ^{65}Zn/^{62}Zn ratio is comparable to values of 0.17% (Zweit et al., 1992) and

0.03% (Bormans et al., 1992) found in previous studies. All other contaminants will

either decay away over the course of processing or will be separated during chemical

processing.

Theoretical production yields were calculated using values of target thickness,

beam current, proton entry energy, and irradiation time listed in previous studies (Table

6). The theoretical yields were compared against experimentally measured yields

reported in their respective studies. Table 18 shows the theoretical yields, experimental

yields for each study.

Table 18. A comparison between measured production yields at EOB from previous
studies and calculated theoretical production yields at EOB.

Reference	Measured Yield	Theoretical Yield	Percent Difference
	(MBq/µA)	(MBq/µA)	(%)
Zweit	206	230	-11
Robinson	74	84	-13
Fukumura	184	168	9
Bormons	141	105	29
Haynes	248	171	37
		Average:	10

It was observed from this comparison that the theoretical yields were an average

of 10% lower than the experimentally reported yields. This was determined to be the

case despite two of theoretical yields having larger values that the reported experimental

yields. There was a lack of quantifiable error reported within the studies investigated. As a result, the best method determined for measuring the accuracy of the calculations was to acquire an average of the percent difference for each study. Given this method, there was a 10% deviation below the experimentally reported yields despite the two outliers.

The 10% deviation is likely attributable to the lack of cGMP applied in producing these generator systems in the previous studies. The practice of cGMP is a federally regulated method of applying quality assurance to generator systems that are produced for the purpose of PET studies. As a result, the irradiation parameters reported in the previous studies may not be entirely accurate, resulting in an experimental production yields that deviate from theoretically predicted values. A Matlab code was written to perform these calculations and can be found in Appendix A. Appendix B holds relevant data used to perform the calculations such as cross-section data, stopping power of protons in copper data, buildup factors, linear attenuation coefficients in lead, mass energy-absorption coefficients in tissue, and gamma-ray energies and yields of the radionuclides.

3.1.2   Alternative Dissolution Method

A foil of high purity natural copper was successfully dissolved in a solution containing 30% hydrogen peroxide (H_2O_2) and 2 M hydrochloric acid (HCl). The dissolution of the copper foil formed a green solution, depicted in Figure 12a, while heated. When the solution was evaporated, it took on a target green color, depicted in Figure 12b. When evaporated to dryness, the copper chloride residue that remained had a

dark brown color, depicted in Figure 12c. This residue was soluble in hydrochloric acid, and could be reconstituted at any concentration of HCl. When reconstituted in 2 M HCl, the solution color returned to a blue hue, depicted in Figure 12d. Additionally, the solution could be shifted back to green when heated or when a stronger concentration of HCl solution was added or shifted back to blue when diluted with additional water.

| (a) | (b) |
| (c) | (d) |
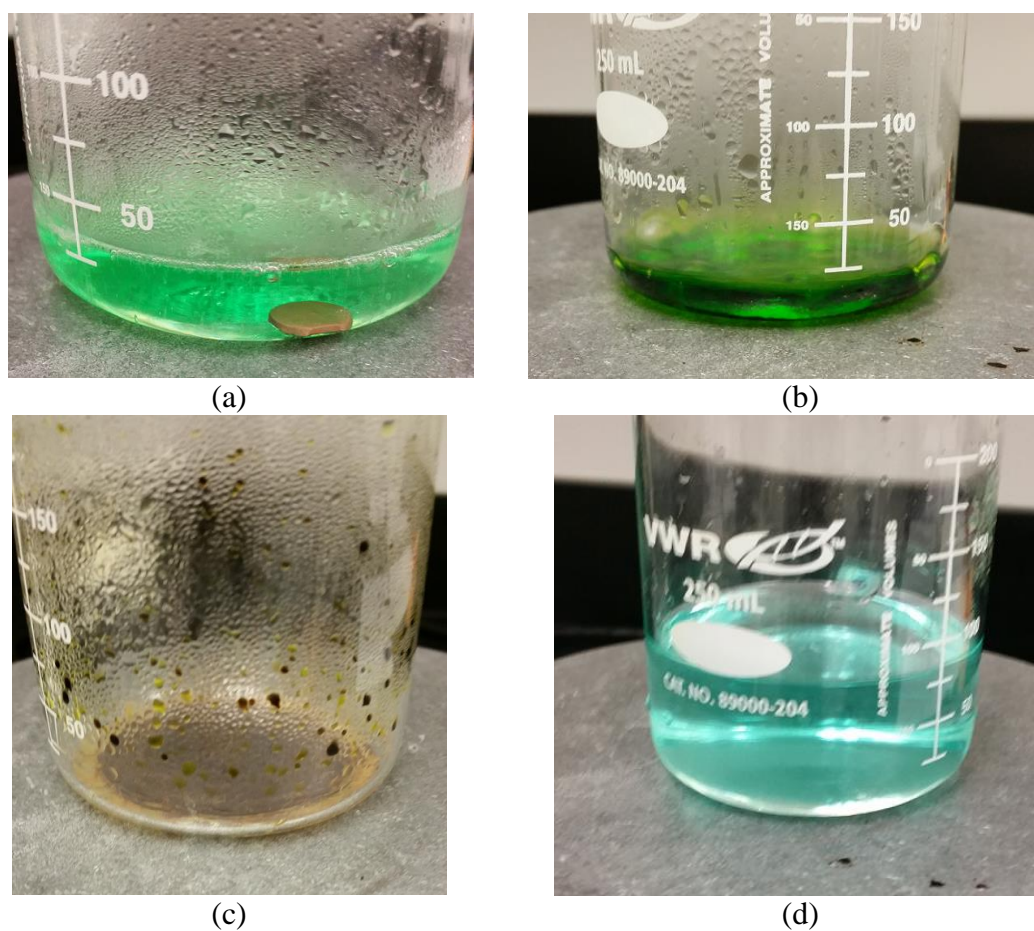
Figure 12. The dissolution process broken into 4 stages. The dissolution of the copper foil (a), evaporating the solution to dryness (b), the residue left after evaporation (c), and the reconstituted 2 M HCl solution after reconstitution (d).

With the successful development of an alternative dissolution method, an alternative target processing procedure was developed. This was carried out with subsequent dissolutions involving the use of a 1.0 mm thick copper foil with a radius of 6.0 mm and average mass of 1.0 g. The focus of the alternative target processing procedure was to reduce the total dissolution time while minimizing the total amount of corrosive chemicals used.

The alternative target processing procedure involved the use of two dissolution vessels. A copper disc was placed within dissolution vessel 1 (DV1) along with 10 ml of 2 M hydrochloric acid pre-heated to 60 ℃. To begin the dissolution process, 1 ml of 30% hydrogen peroxide was added to DV1 and a timer was started. Every 30 seconds after the initial 1 ml of H_2O_2 was added, an additional 1 ml of H_2O_2 was added. This continued until 3.5 minutes had passed and a total of 7.0 ml of H_2O_2 had been added to DV1. The target was left to dissolve for 2.0 minutes while the temperature of the solution peaked at 75 °C. This occurred at approximately 5.5 minutes into the dissolution.

The solution was left to sit until the temperature of the solution began to decrease. This occurred at approximately 6.0 minutes into the dissolution. At this point, the solution in DV1 was transferred to dissolution vessel 2 (DV2), leaving the partially dissolved copper foil in DV1. Immediately, an additional 10 ml of ~60 ℃ 2 M hydrochloric acid was added to DV1. At 6.5 minutes, 1 ml of 30% hydrogen peroxide was added to the solution in DV1 to renew the dissolution of the copper foil. Every 30 seconds, an additional 1 ml of H_2O_2 was added to the solution in DV1. This continued

until 8.5 minutes had passed into the dissolution and a total of 5.0 ml of H_2O_2 has been added to the solution. The solution was left to sit as the copper foil finished completely dissolving.

Complete dissolution occurred at approximately 12.0 minutes after the start of the dissolution. Once completely dissolved, the remaining solution was transferred to DV2. A total of 20 ml of 2 M hydrochloric acid and 12 ml of 30% hydrochloric acid was used to completely dissolve the copper foil. Going into the next phase, the evaporation of the solution occurs in DV2. A flow diagram that outlines this procedure is shown in Figure 13.

While developing the alternative target processing procedure, several key aspects of using 30% hydrogen peroxide were noted. It was observed that when the hydrogen peroxide was added to the solution too quickly or in too large of a quantity, the temperature of the solution increased to over 100 ºC. This would result in the solution boiling over, effectively losing control of the dissolution and spreading the would-be radioactive materials all over the laboratory equipment. Additionally, the rapid increase in temperature also resulted in the simultaneous thermal decomposition of the hydrogen peroxide in the solution. Given this, it was also observed that the temperature of the solution seemed to directly correlate to the hydrogen peroxide available in the solution to dissolve the copper foil. Thus, it was assumed that controlling the temperature of the solution was closely tied to the quantity of hydrogen peroxide and frequency at which it was added to the solution.

0:00	Place copper foil in dissolution vessel 1.
0:00	Add 10 ml of 2M HCl to vessel 1.
0:00	Add 1 ml of 30% H_2O_2 to vessel 1 to start dissolution.
3:30	After 30 seconds, add an additional 1 ml of 30% H_2O_2 to vessel 1. Repeat this until 3.5 min have passed and 7 ml have been added.
6:00	Allow copper foil to sit for 2.5 min. At 6.0 min, transfer solution to dissolution vessel 2.
6:30	Add 10 ml of 2M HCl to vessel 1.
6:30	Add 1 ml of 30% H_2O_2 to vessel 1.
8:30	After 30 seconds, add an additional 1 ml of 30% H_2O_2 to vessel 1. Repeat this until 2.0 min have passed and 5 ml have been added.
12:00	Allow to sit for ~4.0 min. Complete dissolution will occur at ~12 min.

Figure 13. Flow diagram depicting the steps taken in the alternative target processing procedure to achieve a dissolution time of 12 minutes with 30% H_2O_2 and 2 M HCl.

3.1.3 Utilizing LabVIEW

To communicate with a device over a serial connection, a VISA session was opened with the use of the function VISA Open. The computer's serial port was then configured in LabVIEW with the function VISA Serial Port Configuration using the data frame from Table 11. During initialization, the I/O buffer was cleared, flushed, and set to receive and transmit information. Figure 14 shows the code used to open a VISA session and initialize the serial port to communicate with the NE-500 or HEATER-KIT-1LG. The variable VISA resource name is the serial port that the instrument is attached to. This variable is used by each function to identify the port through which the instrument is being used. The function VISA Close was used to end the VISA session once the instrument finished its task. Figure 15 shows the code that was used to close a VISA session.

Figure 14. Opening a VISA session and configuring the serial port.

Figure 15. Closing a VISA session once done with the instrument.

The NE-500 program was designed to be able to control up to three pumps each with an address of 0, 1, and 2, respectively. The program could control a singular pump or multiple pumps in a network. When broken down into components, the program utiliz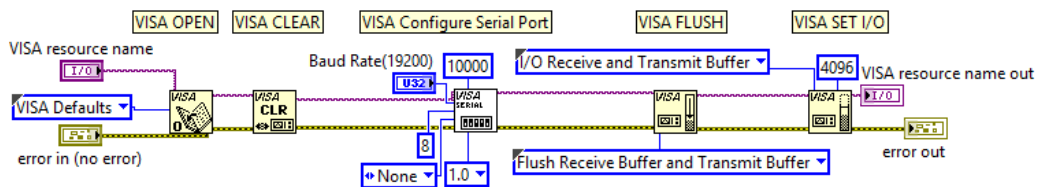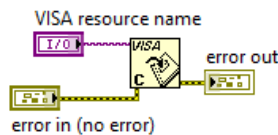ed the following seven functions to communicate with and control the NE-500: initialize serial port, set inner diameter (ID) of syringe, set pumping rate, set volume to be dispensed, run pump, and close serial port.

The program assumed that a B-D 60 ml syringe with an ID of 26.7 mm was loaded onto the NE-500 (Table 8). The code created for the function set inner diameter function is shown in Figure 16. By setting the ID of the syringe to a value greater than 10 mm, all units when dealing with volume are automatically set to ml. The pumping rate was set to 25 ml·min^{-1}, just shy of its maximum pumping rate of 28 ml·min^{-1} (Table 8). The code created for the function set pumping rate is shown in Figure 17. The volume to be dispensed by the NE-500 was designed as an input to be set by the user in the UI during instrument operation. The code created for the function set volume to be dispensed is shown in Figure 18. The activation of the NE-500 was an input to be selected by the user in the UI during instrument operation. The code created for the function run pump is shown in Figure 19.

The program takes each of these parameters and passes the command along to the pump sequentially by using the function VISA write. A wait function was used to pause the program for 50 milliseconds after each VISA write function was executed. This pause allows the instrument sufficient time to process the command. When a command has been successfully processed, the common response from the pump will be

00X, where 00 is the instrument's address and X is some combination of ASCII

characters interpreted as an instrument response. The function VISA read (Figure 20)

was utilized to acquire the instrument response and display it to the user.
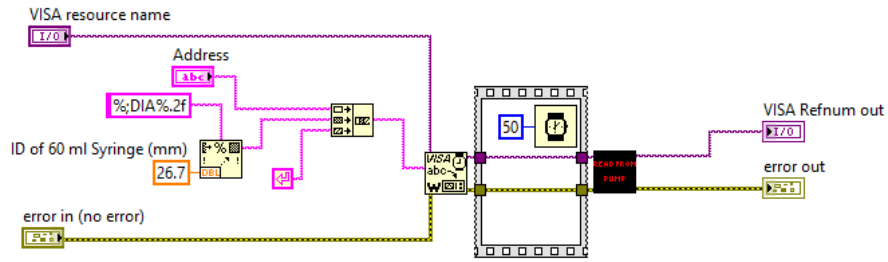
Figure 16. Using the DIA command to set the ID of the syringe.
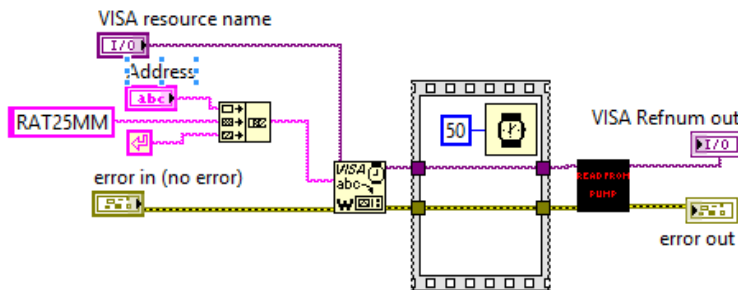
Figure 17. Using the RAT command to set the pumping rate to 25 mm·min^{-1}.
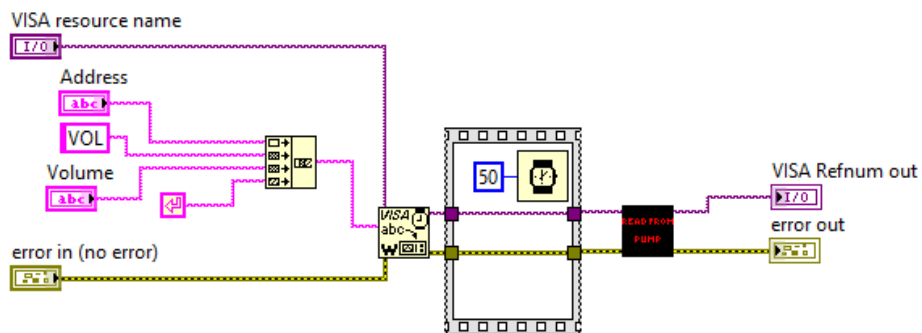
Figure 18. Using the VOL command to set the dispensing volume with an input set by
the user.
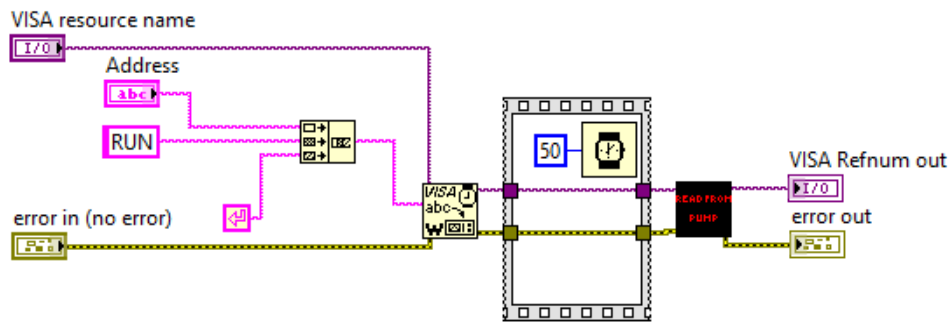
Figure 19. Using the RUN command to start the pump.
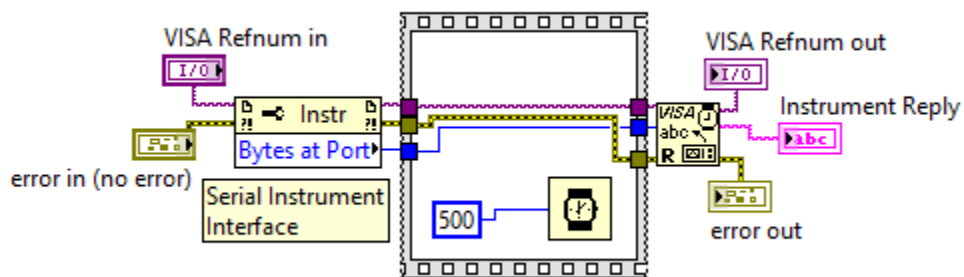
Figure 20. Using the VISA read function to read the instrument response and display it to the user through the variable Instrument Reply.

The HEATER-KIT-1LG program was designed to be able to control up to two heaters each with an address of 3 and 4, respectively. The program could control a singular heater or a heater connected into the same network as the NE-500 pumps. When broken down into components, the program utilized the following seven functions to communicate with and control the HEATER-KIT-1LG: initialize serial port, set heater setpoint, set heater units, start heater, query heater temperature, stop heater, and close serial port. The program sets the heating setpoint to a pre-determined temperature that acts as a constant within the programming. The code created for the function set heater

setpoint is shown in Figure 21. The temperature of the heater was set to 110 °C with this

function. The code created for the function set heater units is shown in Figure 22. The

activation of the HEATER-KIT-1LG was designed as an input to be set by the user in

the UI during instrument operation. The code created for this function is identical to

Figure 19. While the instrument was activated, the program began a timer and

continuously queried the temperature of the heating pad from the instrument (Figure 20).

The code created for the function query heater temperature is shown in Figure 23. The

deactivation of the HEATER-KIT-1LG was designed as an input to be set by the user in

the UI during instrument operation. The code created for the function stop heater is

shown in Figure 24.
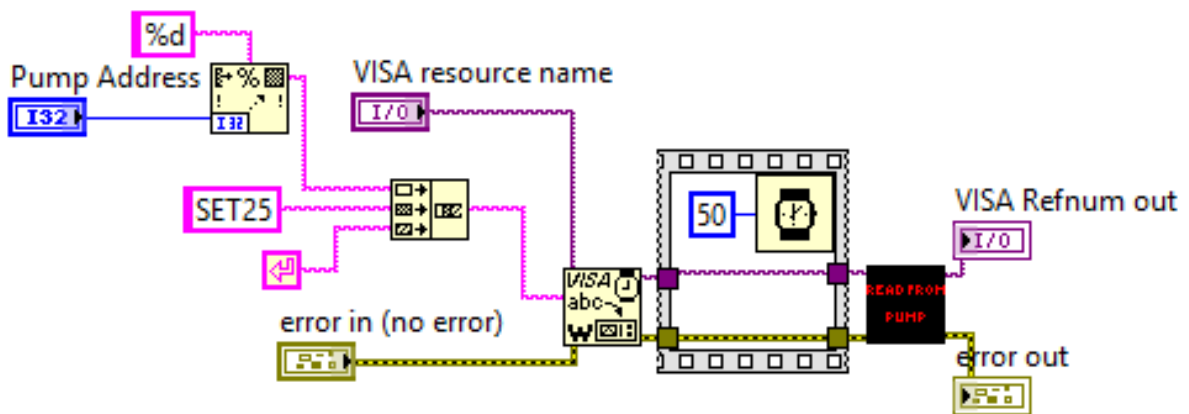
Figure 21. Using the SET command to set the heating setpoint.
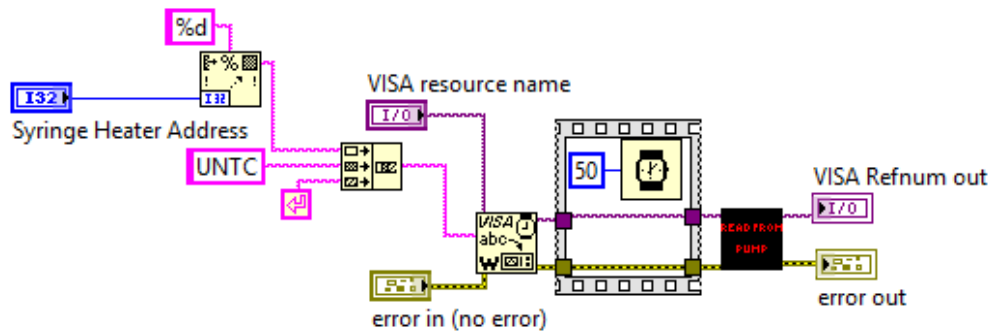
Figure 22. Using the UNT command to set the units to Celsius.
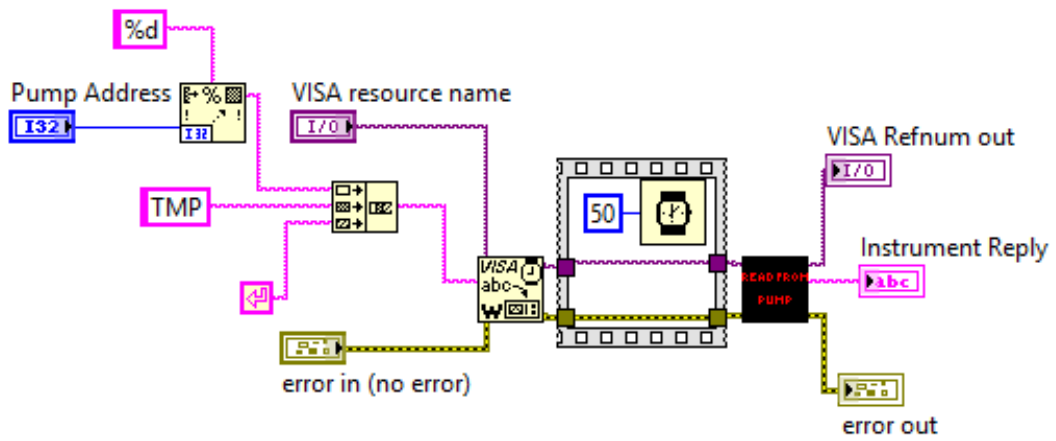
Figure 23. Using the TMP command to query the current temperature of the heating pad.
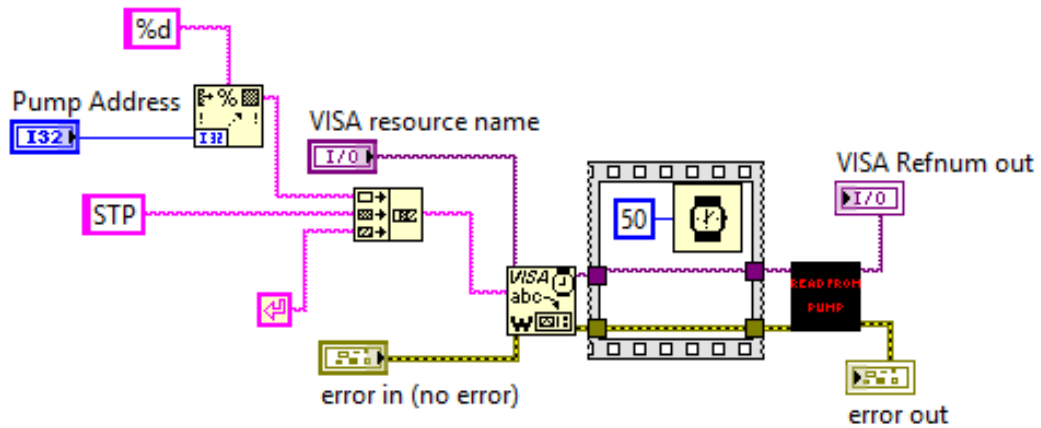
Figure 24. Using the STP command to deactivate the heater.

59

The USB-6501 program can only control one device at a time. This device did not require an address because it was not part of a network. The UI organizes the 24 channels into 3 different ports, labeled 0-2, with eight channels each, labeled 0-7. The labels for all ports and channels were labeled to conveniently correspond with the pin assignments on the physical device (Table 9). It was designed such that each channel in the UI had its own trigger switch that could be triggered by the user during normal instrument operation. The trigger switch had a true/false value that dictated the on/off state of its channel, respectively. When triggered by the user, an LED indicator next to the channel was designed to provide visual confirmation for the on/off state of the channel.

Each of the three ports were arranged into their own array. These arrays held the true/false values for each of the trigger switches. A looping algorithm was utilized to check each of the true/false values for each of the 8 channels in each port. Two things occurred after this point. First, if true the LED indicator for that trigger switch was turned on and if false, the LED indicator was turned off. Second, the true/value values for each trigger switch were sequentially placed back into an array that was passed to the DAQ Assistant. The DAQ Assistant will take these inputs for each port and automatically generate code that applies the inputs to the USB-6501 and change the physical state of each respective channel.

Figure 25 shows the code for implementing this described method of controlling the USB-6501. To verify that the program successfully controlled the USB-6501, an experiment with LED's was conducted. A simple circuit was constructed with the use of

60

24 LED's where red, yellow, and green correspond to ports 0, 1, and 2, respectively.

Figure 26 shows the results of this experimental setup. Figure 27 shows a simultaneous

view of the UI of the program used to control this experimental set. Upon close

inspection, it can be observed that the active or green LED channels in the USB-6501

program correctly matched the lit LEDS of experimental setup.
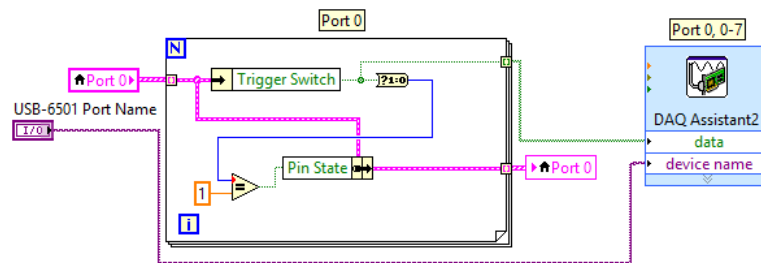
Figure 25. The code used to implement the DAQ Assistant in controlling channels 0-7
on Port 0 of the USB-6501.
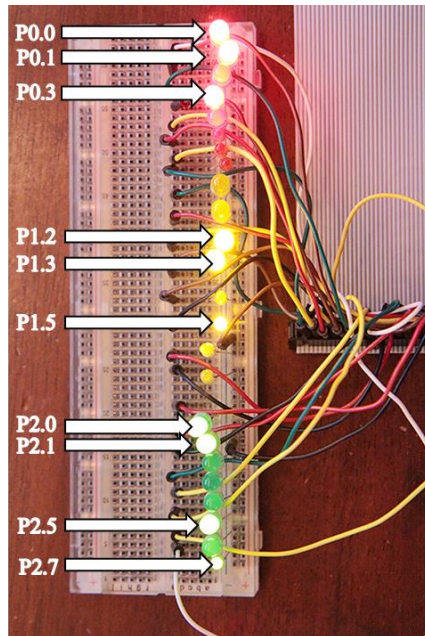
Figure 26. Each LED is attached to a channel on the USB-6501. The ports 0, 1, and 2 are
red, yellow, and green, respectively. The lit LEDs correspond to the active channels in
Figure 27.

61
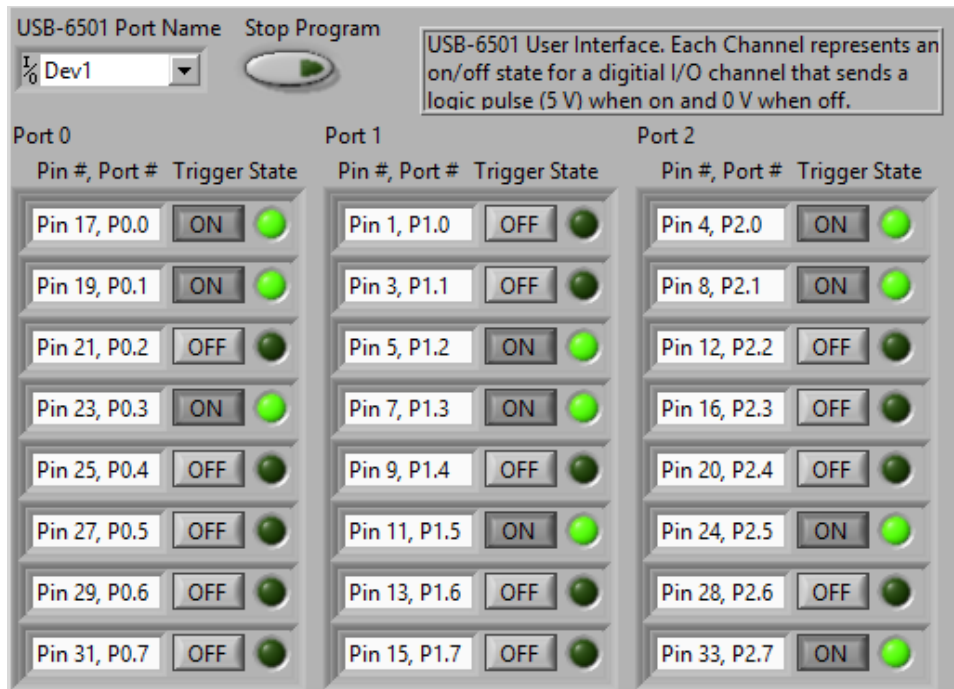
Figure 27. The USB-6501 program that is controlling the 24 LEDs found in Figure 26. Each active channel corresponds to a lit LED.

A fourth program was developed to manually assign an address to any instrument directly connected to the computer. This was done by initializing the serial port, selecting a numerical address, using the ADR command with VISA write to send the address to the instrument, and closing the serial port. The programming is nearly identical to that shown previously for the other programs. This program was necessary to set addresses to instruments prior to being placed in a network.

3.2 Discussion

3.2.1 Optimizing ^{62}Zn Production

The maximum proton entry energy considered relevant towards producing ^{62}Zn while minimizing the yield of other contaminants is 30 MeV. With an proton entry energy of 30 MeV, a copper foil thickness of 1.0 mm will result in a proton exit energy of 17.14 MeV. Between 17.14 and 13.6 MeV, the cross-section for the ^{63}Cu(p,2n) reaction goes from approximately 40 to 3 mb, respectively. To reduce the energy of the proton beam to below the 13.6 MeV threshold for the ^{63}Cu(p,2n) reaction, a copper foil thickness of 1.2 mm is required. Given the small reaction cross-section area available between 1.0 and 1.2 mm, the average difference in ^{62}Zn yield between these two thicknesses is less than 6%. Beyond 1.2 mm, any increase in ^{62}Zn yield is negligible due to the proton beam being reduce to a level below the necessary threshold energy of 13.6 MeV. Given that the increase in ^{62}Zn yield is marginal between 1.0 and 1.2 mm, it was determined that the optimal target thickness was 1.0 mm.

Given that copper is a transition metal, all resulting contaminants are also transition metals. The chemical differences between the product and contaminants allow for easy separation with little difficulty. Given that the contaminants pose little concern towards the radionuclide purity of the final product, their primary concern comes from the necessary decay of the short-lived contaminants to safely handle the irradiated target after EOB. Thus, estimating the radiation exposure from the target at EOB provided the best method for determining how the entry energy affected the production of contaminants and more importantly, how it affected the cooling period.

Table 16 shows the dose equivalent rates calculated for each radionuclide, the total dose equivalent rate from the target for proton entry energies between 18 and 30 MeV. The results show that the short-lived contaminants, ^{63}Zn and ^{61}Cu, contribute entirely to the radiation exposure field around the target. For entry energies between 18 and 27 MeV the cooling period is 2 hours and between 28 and 30 MeV it is 1 hour. The decrease in cooling period at higher energies is due to the reduction in the production of ^{63}Zn. While ^{61}Cu is produced in a greater quantity at the higher energies, it contributes less to the radiation exposure around the target than ^{63}Zn. Additionally, the copper contaminant can easily be separated during chemical processing and does not affect the radionuclide purity of ^{62}Zn.

The respective cooling periods were used to decay correct the EOB production yields for all radionuclides (Table 17). This revealed a peak in the production yield of ^{62}Zn at a proton entry energy of 29 MeV. Given these results, the optimal proton entry energy for maximizing the production yield of ^{62}Zn is 29 MeV. Given these parameters, the maximum production yield calculated for ^{62}Zn was 175 MBq·μA^{-1}·h^{-1} (Table 17). Correcting for the 10% deviation from experimental measurements and accounting for an additional hour of decay due to processing, the maximum potential yield was between 160 and 180 MBq·μA^{-1}·h^{-1}.

This value represents the activity that is expected to be loaded onto a generator column after processing. According to Zweit et al., 1992, it is common for 2.0 GBq to be loaded onto the generator column and hold a sufficient shelf-life of 24-48 hours (Zweit et al., 1992). Given this, a beam current as low as 15 μA·hr would be sufficient to

produce a generator with a ^{62}Zn activity of 2.4 GBq. Thus, it was determined that 160

MBq·µA^{-1}·h^{-1} could feasibly provide a generator system with a comparable shelf-life to

the standard with a moderate beam current and irradiation time.

3.2.2   Alternative Target Processing Procedure

During the various stages of the dissolution of the copper foil with the 30%

hydrogen peroxide and 2 M hydrochloric acid, various color changes of the solution

were observed. The color changes were attributable to the copper(II) ions that were

displaced into the solution during dissolution. The two colors blue and green were

observed in the solution. The blue color is attributable the presence of the

hexaaquacopper(II) ion, $[Cu(H_2O)_6]^{2+}$, that is formed when copper(II) ions are in

aqueous solution (Rayner-Canham and Overton, 2003). The green color is attributable to

the presence of the tetrachlorocuprate(II) ion, $[CuCl_4]^{2-}$, that is formed when copper(II)

ions are in an aqueous solution containing a high concentration of chloride ions (Rayner-

Canham and Overton, 2003). When diluted, the green solution will shift back to a blue

solution. When a stronger concentration of hydrochloric acid was added to the solution,

the blue solution shifted back to green.

This illustrated a clear demonstration of Le Châtelier's principle, which describes

how the chemical dynamic equilibrium between the formations of different compounds

shifts when conditions such as concentration or temperature are changed. In the case of

the observed color changes with the aqueous solution containing copper(II) ions, the

color shifted towards the formation of one copper complex or the other when these exact

conditions were changed. When water is added to the solution, the concentration of the chloride ions is diluted resulting in an equilibrium shift (Equation 4) to the right and a subsequent increase in the formation of hexaaquacopper(II) ions. When the concentration of chloride ions in the solution was increased, the excess Cl⁻ shifted the equilibrium (Equation 4) to the left resulting in an increase in the formation of tetrachlorocuprate(II) ions. These equilibrium shifts were responsible for the color changers to blue and green, respectively. This is most clearly illustrated with Equation 4 (Rayner-Canham and Overton, 2003).

$$[CuCl_4]^{2-}_{(aq)} + 6\,H_2O_{(l)} \rightleftharpoons [Cu(H_2O)_6]^{2+}_{(aq)} + 4\,Cl^-_{(aq)} \qquad (4)$$
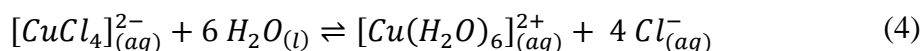
The results from the final solution obtained in Figure. 12d indicate that the hexaaquacopper(II) ion is formed in a 2 M HCl solution due to the blue color. Given that the chemical processing phase utilizes anion exchange chromatography to separate ^{62}Zn from the contaminants using their chloride complexes (Bormans et al., 1992; Robinson Jr et al., 1980) , the hexaaquacopper(II) ion in 2 M HCl is likely the correct copper(II) ion for chemical separation.

The objective in developing this alternative dissolution method was to reduce the volume of corrosive fumes generated during target processing. Given the concentration of hydrogen peroxide, the continued presence of lower concentration HCl, and the temperatures reached during dissolution, it cannot be said confidently that this objective was achieved without performing further experiments that provide evidence to support

66

such claims. However, it is reasonable to assume that the volume of corrosive fumes generated during target processing with the alternative method are reduced relative to the conventional one. The number of chemical steps involved to dissolve the copper target and form the chloride complexes are reduced from 3 with the conventional method to 1 with the alternative method. The quantity in which the corrosive fumes are reduced or eliminated with the alternative dissolution method will have to be measured in future studies.

The feasibility of implementing the alternative dissolution method into the overall generator production procedure was based upon achieving a dissolution time comparable to that of the conventional procedure. The use of concentrated acids result in the rapid dissolution of a copper target. The term rapid was never quantified in any of the previous studies, but it was interpreted that the dissolution time occurred on a time frame that did not impact the overall processing time of the generator system. Thus, it was assumed that conventional dissolution times were on average 2 minutes. With an average generator processing time of 60 minutes (Zweit et al., 1992), the conventional target processing procedure takes up 4% of the total processing time. Given this, the primary goal was to produce a alternative target processing procedure with the alternative dissolution method that could provide a comparable dissolution time that comprised approximately 4% of the total processing time.

It was determined that the best method for optimizing the use of hydrogen peroxide during the dissolution was to monitor the temperature of the solution. Due to the exothermic nature of the decomposition of hydrogen peroxide, it was assumed that

the temperature of the solution directly correlated to the amount of hydrogen peroxide available for dissolution of the copper foil. Preliminary experiments showed that the addition of hydrogen peroxide in either large quantities at one time or in small quantities too quickly resulted in an exponential increase of solution temperature. This led to the inefficient thermal decomposition of the hydrogen peroxide before it could dissolve the copper foil. It was quickly realized that the addition of hydrogen peroxide had to be controlled in a manner that reduced its thermal decomposition throughout the dissolution.

To completely dissolve a 1.0 g copper foil, 1.6 ml of 30% hydrogen peroxide is required. The use of large quantities of 30% hydrogen peroxide was discarded for a more favorable use of smaller quantities that were both adequate in completely dissolving the copper foil while simultaneously allowing for a better method in controlling the temperature of the solution. By incrementing the addition of hydrogen peroxide over set time intervals, fresh hydrogen peroxide is consistently added to the solution over a time frame that does not drastically impact the temperature of the solution. This method effectively minimized the thermal decomposition of hydrogen peroxide before it could react with the copper foil to dissolve it.

The alternative target processing procedure was detailed in the results and is summarized in Figure 13. A total of 12.0 ml of 30% hydrogen peroxide was used to dissolve the copper foil with the alternative procedure, and was added in increments of 1.0 ml. This is significantly more than the 1.6 ml required to completely dissolve the copper foil. The decision to use this amount was based on the difficulty in quantifying

how much hydrogen peroxide is actually lost through thermal decomposition during dissolution. Thus it was decided that a conservative amount of hydrogen peroxide should be added in each increment while maintaining a sufficiently small volume to remain in control of the solution temperature.

Using this method, the solution temperature peaked at approximately 75 °C after adding 7 ml of hydrogen peroxide over 3.5 minutes to the solution. The solution remained at this temperature for an additional 2.5 minutes after the last ml of hydrogen peroxide had been added. A decrease in temperature indicated that the solution needed to be refreshed with additional hydrogen peroxide. However, the temperature decreased at such a slow rate that any additional hydrogen peroxide added to the solution at that point would quickly raise the temperature above 75 ºC. To achieve a more effective control of the solution's temperature, the solution in DV1 was completely transferred to DV2. This allowed for the fresh addition of hydrochloric acid and hydrogen peroxide to DV1 to continue dissolution of the partially dissolved copper foil. This essentially resets the temperature of the solution and allows for a less restricted addition of hydrogen peroxide in the second half of the procedure.

This resulted in the addition of 5.0 ml of hydrogen peroxide over 2.0 minutes where the solution temperature peaked right under 70 °C. The copper foil was left to completely dissolve after this point. It is worth noting that 16 ml of 2 M HCl is required to completely dissolve a 1.0 g copper foil. A conservative 20 ml of 2 M HCl was utilized with this procedure where 10 ml was added at the start and again after the entire solution is refreshed. To put this in perspective, the conventional method typically utilized 25 ml

of hot 16 M HNO_3 and 25 ml of 12 M HCl completely dissolve the copper target and form the chloride complexes (Robinson Jr et al., 1980; Zweit et al., 1992).

With the alternative target processing procedure outlined in Figure 13, an average dissolution time of 12 minutes was achieved. Assuming a normal dissolution time of 2 minutes, this adds approximately 10 minutes to the 60 minute total processing time, extending it to 70 minutes. As a result, the alternative target processing procedure would consist of 17% of the total 70 minute processing time. Thus, the alternative target processing procedure did not meet the goal of comprising only 4% of the total processing time. However, this dissolution time is still considered very promising.

The current alternative procedure leaves considerable room for further optimization. The use of a glass thermometer provided a sufficient measurement of the solution's temperature for the purpose of reducing the dissolution time to a reasonable time frame. But, it lacked the necessary accuracy and temperature response to properly optimize the use of the hydrogen peroxide. With the use of a more sensitive temperature sensor and the utilization of a more precise method of delivering hydrogen peroxide to the solution, dissolution times could be reduced to less than 10% of the total processing time with the alternative target processing method. However, it is worth noting that regardless of the room for further optimization, a 70-minute processing time still remains viable when producing a generator system whose parent has a half-life of 9.186 hours.

3.2.3   Automating Procedural Processes

Four unique programs were developed in LabVIEW to remotely control the NE-500 (Figure 28), HEATER-KIT-1LG (Figure 29), and USB-6501 (Figure 30) through a computer interface. The fourth program was designed to assign an address to any instrument directly connected to the computer (Figure 31). The three programs were developed as a proof of concept that demonstrated the feasibility in controlling each of the three instruments through a remote-controlled interface. As a result, the development of these programs did not take into account any major error checking that would be required to be in compliance with any good manufacturing practices. Flow diagrams that depict the logic behind each program are shown in Appendix C.

Each of the three programs successfully automate the specific tasks given to each instrument, but only provide a means of semi-automating the overall generator production procedure. The goal was to provide a proof of concept that illustrated the feasibility in automating the overall generator production procedure. When discussing automation in this context, it can be defined as the complete automation of every step of generator production from start to finish without a requirement for any user input during operation. The use of three unique programs, all of which require user-input at critical junctions, to complete separate tasks throughout the procedure understandably fall short of full automation. However, they provided several useful results.
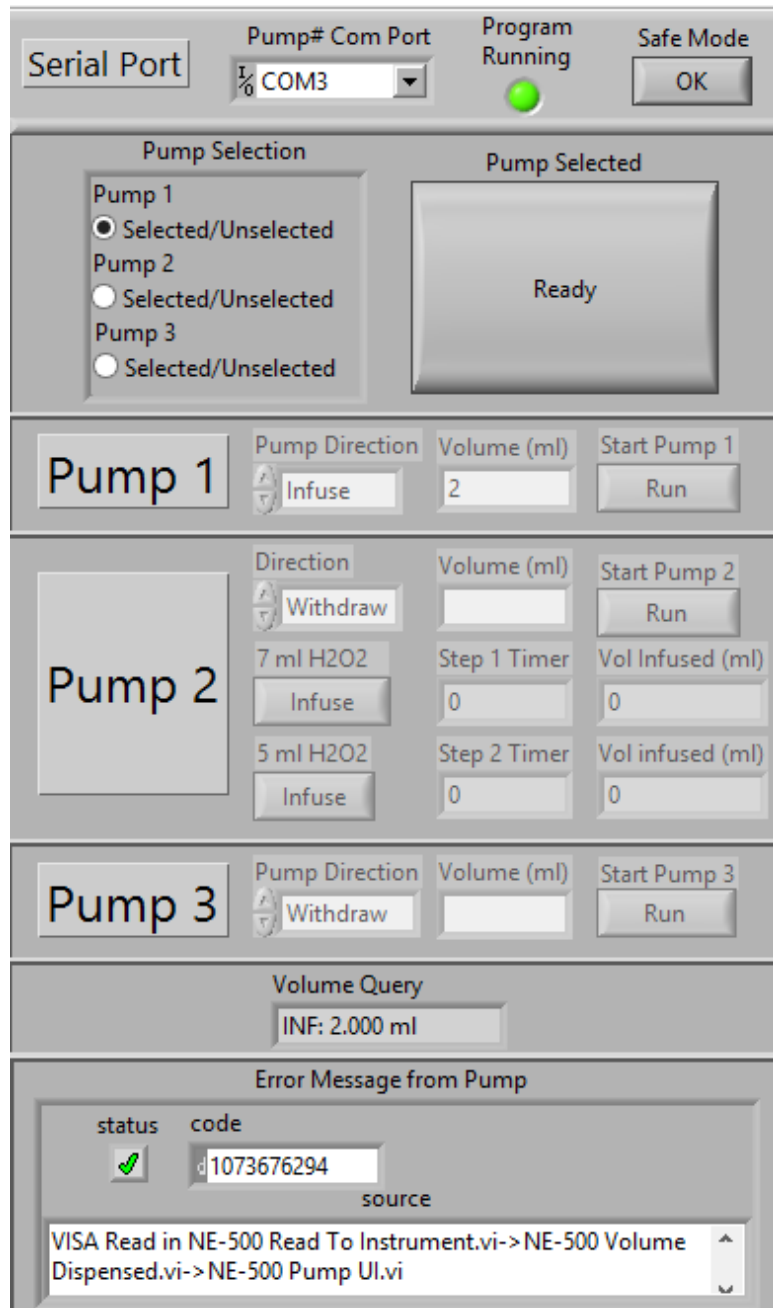
Figure 28. The user interface for the program that controls the NE-500.
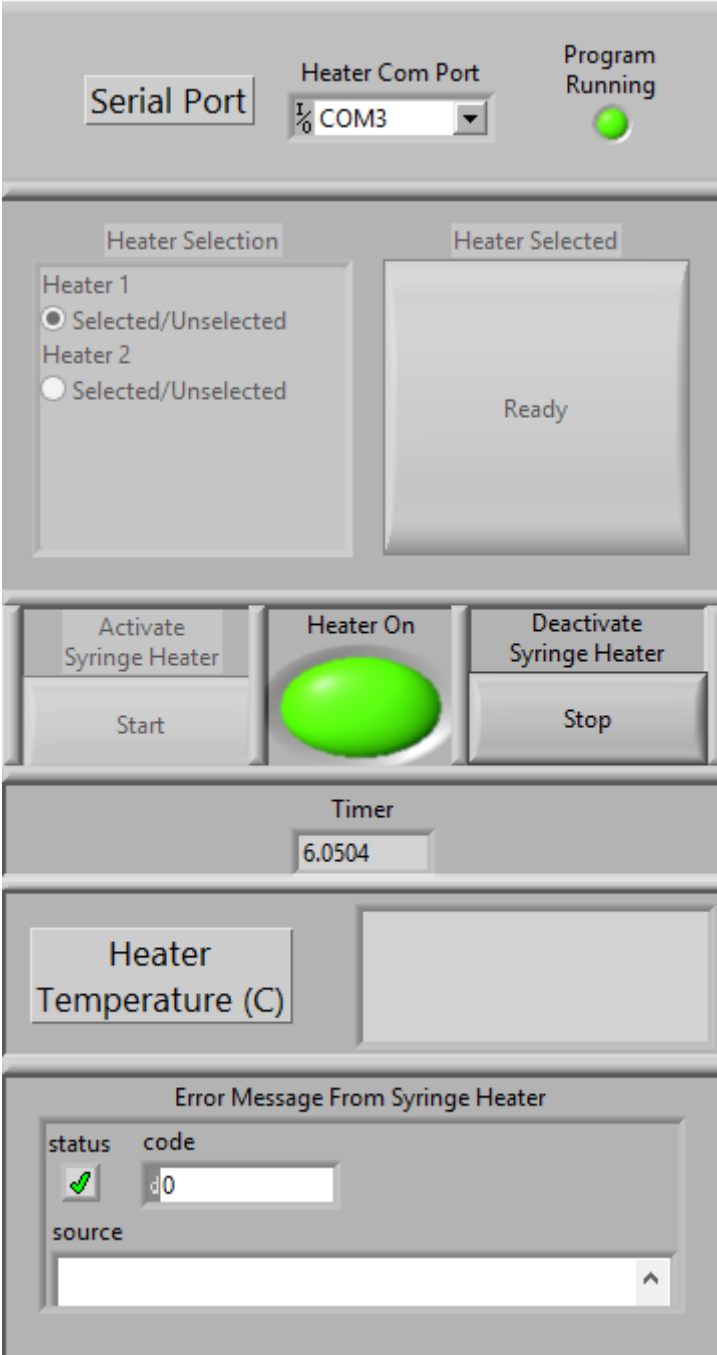
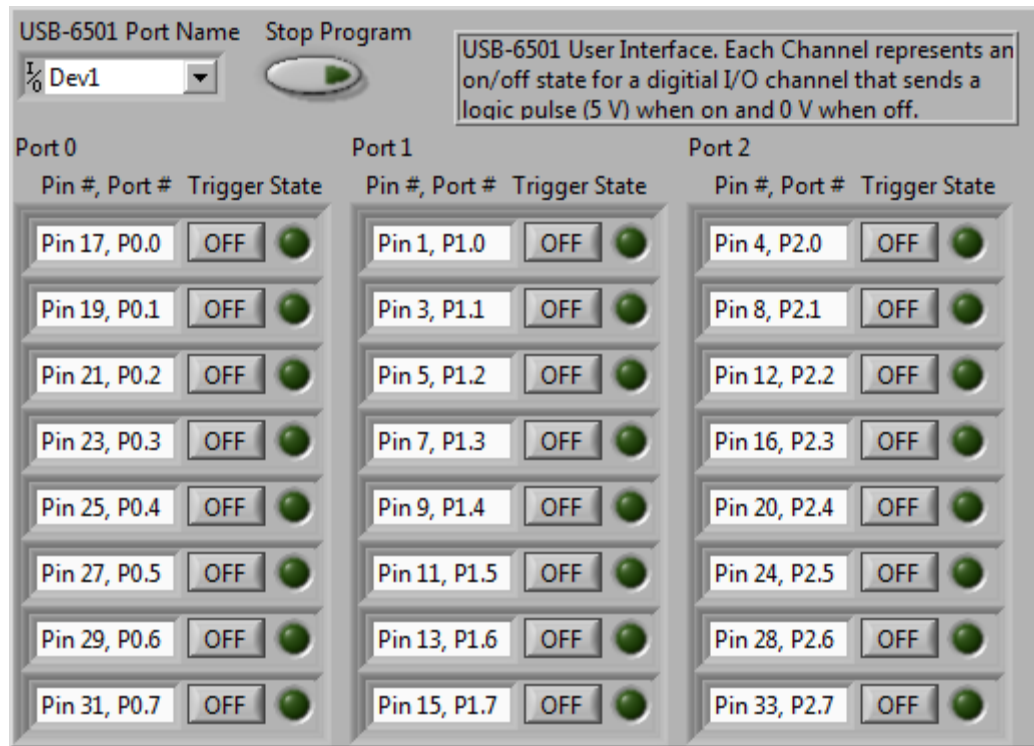Figure 29. The user interface for the program that controls the HEATER-KIT-1LG.

Figure 30. The user interface for the program that controls the USB-6501.
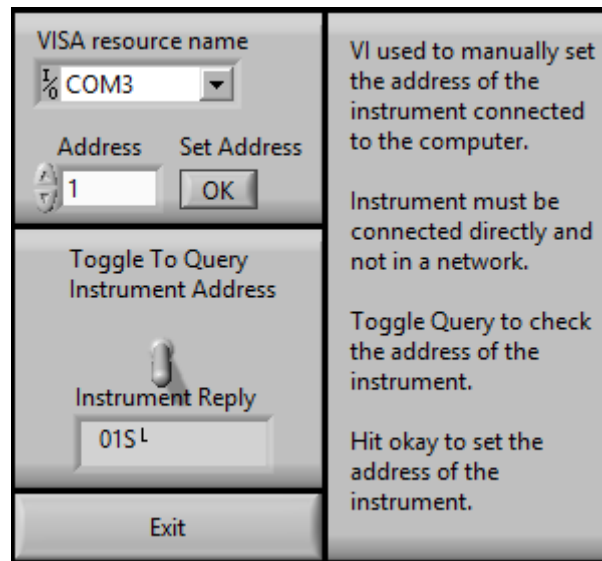
Figure 31. The user interface for the program that assigns addresses to instruments.

Firstly, it was discovered that LabVIEW could be used to successfully control the instruments. Figures 14-25 illustrate very clearly how LabVIEW is utilized to control the instruments and sufficiently provide a foundation to design more complex programs around. Secondly, the use of separate programs was a simple method of illustrating that multiple instruments could be used simultaneously. For example, the HEATER-KIT-1LG program could heat a solution simultaneously while fluids were transferred from one vessel to another with the NE-500 program. Thirdly, a small portion of the procedure outlined in Figure 13 was fully automated in the NE-500 Program. The addition of hydrogen peroxide was broken up into total volumes of 7 ml during the first half of the procedure and 5 ml during the second half. Once the program has acquired an input from the user, it will start a timer, add 1 ml of hydrogen peroxide, and continue to add an additional 1 ml every 30 seconds until 7 ml has been added. The program will then wait for an additional 2.5 minutes before it requests another input from the user to proceed to the next step. The same sequence of steps will occur for adding 5 ml of hydrogen peroxide as well. A timer is visible throughout the automated sequence to provide the user with a visual indication of progression of the procedure. This showcased the feasibility in implementing more complex, automated algorithms utilizing the instrument control functions outlined in Figures 14-25.

These results provide a successful proof of concept for the feasibility in creating a system that can automate the production of the $^{62}Zn/^{62}Cu$ generator systems. Incorporating all these different results into one program is the next logical step towards producing a software that is capable of total automation. This will require characterizing

very well every single step of the overall generator production procedure, isolating all constants, and ensuring variables that fluctuate remain within expected levels. The system itself will ideally adopt a modular design. This design criteria went into the decision behind purchasing each of the three instruments. They are either compact or purchased as an OEM version which include mountable chasses for the feasible implementation into a modular system. The use of modular is intended to imply that the system will be self-contained and capable of operating regardless of its location. This gives the system a measure of flexibility in its implementation.

4. SUMMARY AND RECOMMENDATIONS

4.1 Conclusion

The purpose of this study was to provide a foundation for mass producing ^{62}Zn/^{62}Cu generator systems. Firstly, this was approached by developing a method that considered all irradiation parameters. It was identified that the target thickness and proton entry energy impacted the production yield of ^{62}Zn the greatest. The optimal target thickness and proton entry energy for maximizing the production of ^{62}Zn is 1.0 mm, and 29 MeV, respectively. Using estimated radiation exposure values for these parameters, the cooling period for the target was calculated to be 1 hour. A maximum theoretical ^{62}Zn yield of 160 MBq·µA^{-1}·h^{-1} after the 1 hour cooling period was calculated. The ^{65}Zn/^{62}Zn ratio was calculated to be 0.3% at proton entry energies of 29 MeV. Conveniently, despite the use of a smaller target, theoretically equivalent production yields can be achieved with 29 MeV protons. This is an energy well suited for a medium energy cyclotron.

Secondly, an alternative target processing method was developed that successfully dissolved a copper foil with the use of 30% hydrogen peroxide and 2 M hydrochloric acid. This alternative method ideally reduces or eliminates entirely the total amount of corrosive fumes generated during the target processing phase. Eliminating or simply reducing the volume of corrosive fumes will effectively reduce the damage delivered to the equipment in radiochemistry facilities as a direct result of dissolving the irradiated copper target. The color of the solution was used to determine that the copper(II) ions had correctly formed the hexaaquacopper(II) ion in a 2 M HCl solution

necessary for separation from ^{62}Zn. Additionally, an alternative target processing procedure was developed with this method that yielded a dissolution time of 12 minutes. This dissolution time consisted of approximately 17% of an overall processing time of 70 minutes. Given this, it can be determined that a generator production procedure that implements the alternative target processing method would be better optimized towards routinely producing ^{62}Zn/^{62}Cu generator systems.

Thirdly, software was developed in LabVIEW for controlling specific instruments for the purpose of showing that the generator production procedure could be automated. The instruments NE-500, HEATER-KIT-1LG, and USB-6501 were utilized to automate the transfer of fluids, heating of solutions, and electronic manipulation of valves, respectively. The software was able to successfully demonstrate that the hardware components were successfully controlled with LabVIEW and performed their roles as intended. Specific instructions were created on how to control the three instruments with LabVIEW and can be utilized to develop a more complex program with the intent to fully automate the entire production process. The instruments, NE-500 and USB-6501, purchased as OEM versions both have mountable chassis' that can feasibly be implemented into a modular system. The HEATER-KIT-1LG was not purchased as an OEM version, but maintains dimensions that are small enough to be implemented into a modular system with some innovative engineering.

4.2   Future Work

Future work will involve verifying, optimizing, and implementing the results of this study towards the routine production of ^{62}Zn/^{62}Cu generator systems. The first step is verifying that the volume of corrosive fumes generated with the alternative target processing method have been Eliminated. If they have not been eliminated effectively, their quantity should be measured to provide an estimate of the expected damage to be incurred on equipment due to target processing in a radiochemistry facility.

The second step will be in establishing and optimizing the production of ^{62}Zn. It should be determined if a ^{62}Zn production yield of 180 MBq·μA^{-1}·h^{-1}is not just theoretically possible but physically as well. The production runs should also establish what the ideal beam current and irradiation time should be, as both are subject to manipulation according to the size of the target. Next, the alternative target processing procedure should be optimized to reduce the total dissolution time to below 10 minutes. Currently, this procedure will add an additional 10 minutes to the total processing time. It is worth the effort to optimize this method to achieve better dissolution times.

Lastly, the proof of concept showed that automating the generator production process with the use of a remote controlled modular system was possible. There are three important steps following this study that must be taken. The first is to characterize the generator production procedure very precisely. The second is to take this information and develop a new LabVIEW program that incorporates all of the instruments into one interface. This program should be capable of fully automating the production procedure from start to finish without the need for any user input. The third step is to develop a

physical prototype of the system. This will be crucial for troubleshooting and testing the

LabVIEW program as LabVIEW cannot provide any simulated results. Instead, it must

be attached to physical instruments or hardware to provide feedback on any software that

is being developed.

REFERENCES

Agency, I.A.E., 2009a. Cyclotron produce radionuclides: guidelines for setting up a facility, Technical reports series (International Atomic Energy Agency) ; no. 471. Technical Reports Series, Vienna : International Atomic Energy Agency.

Agency, I.A.E., 2009b. Cyclotron produced radionuclides: princples and practice, Technical reports series (International Atomic Energy Agency) ; no. 465. Tech. Rep, Vienna : International Atomic Energy Agency

Bailey, D.L., Townsend, D.W., Valk, P.E., Maisey, M.N., 2005. Positron emission tomography. Springer.

Beanlands, R., Muzik, O., Mintun, M., Mangner, T., Lee, K., Petry, N., Hutchins, G.D., Schwaiger, M., 1992. The kinetics of copper-62-PTSM in the normal human heart. Society of Nuclear Medicine 33, 684-690.

Bilewicz, A., 2006. Separation of Sr-82 from rubidium target for preparation of Sr-82/Rb-82 generator. Journal of Radioanalytical and Nuclear Chemistry 268, 485-487.

Blower, P., Blower, J., Lewis, J., 1996. Copper radionuclides and radiopharmaceuticals in nuclear medicine. Nuclear Medicine and Biology 23, 957-980.

Bormans, G., Bormans, A., Janssen, P., Adriaens, D., Crombez, A., Witsenboer, J., de Goeij, L., Mortelmans, A., 1992. A 62Zn/62Cu generator for the routine production of 62Cu-PTSM. International Journal of Radiation Applications and Instrumentation. Part A, Applied radiation and isotopes 43, 1437-1441.

Coleman, R.E., 1988. Positron emission tomography: clinical status in the United States in 1987. The Journal of Nuclear Medicine 29, 1136-1143.

Fujibayashi, Y., 1989. A new zinc-62/copper-62 generator as a copper-62 source for PET radiopharmaceuticals. The Journal of Nuclear Medicine 30.

Fujibayashi, Y., 1990. 62 Cu-labeling of human serum albumin-dithiosemicarbazone (HSA-DTS) conjugate for regional plasma volume measurement: Application of new 62 Zn/ 62 Cu generator system. Chemical and Pharmaceutical Bulletin 38, 1946-1948.

Fukumura, T., 2006. An improved 62Zn/62Cu generator based on a cation exchanger and its fully remote-controlled preparation for clinical use. Nuclear medicine and biology 33, 821-827.

Green, M.A., 1987. A potential copper radiopharmaceutical for imaging the heart and brain: Copper-labeled pyruvaldehyde bis(N4-methylthiosemicarbazone). International Journal of Radiation Applications and Instrumentation. Part B. Nuclear Medicine and Biology 14, 59-61.

Green, M.A., Klippenstein, D.L., Tennison, J.R., 1988. Copper (II) bis (thiosemicarbazone) complexes as potential tracers for evaluation of cerebral and myocardial blood flow with PET. J Nucl Med 29, 1549-1557.

Green, M.A., Mathias, C.J., Welch, M.J., McGuire, A.H., Perry, D., Fernandez-Rubio, F., Perlmutter, J.S., Raichle, M.E., Bergmann, S.T., 1990. Copper-62-labeled pyruvaldehyde bis(N sup 4 -methylthiosemicarbazonato)copper(II): Synthesis and evaluation as a positron emission tomography tracer for cerebral and myocardial perfusion. Journal Name: Journal of Nuclear Medicine; (United States); Journal Volume: 31:12, Medium: X; Size: Pages: 1989-1996.

Grütter, A., 1982. Excitation functions for radioactive isotopes produced by proton bombardment of Cu and Al in the energy range of 16 to 70 MeV. Nuclear Physics A 383, 98-108.

Gul, K., 2001. Calculations for the excitation functions of the 63Cu(p,n)63Zn, 63Cu(p, 2n)62Zn and 65Cu(p,n)65Zn reactions. Applied Radiation and Isotopes 54, 147-151.

Haddad, P.R., 1994. Ion chromatography. Handbook on Metals in Clinical and Analytical Chemistry, 135.

Haynes, N.G., Lacy, J.L., Nayak, N., Martin, C.S., Dai, D., Mathias, C.J., Green, M.A., 2000. Performance of a 62Zn/62Cu Generator in Clinical Trials of PET Perfusion Agent 62Cu-PTSM, Journal of Nuclear Medicine, pp. 309-314.

Keppler, J.S., Conti, P.S., 2001. A cost analysis of positron emission tomography. American Journal of Roentgenology 177, 31-40.

Kraus, K.A., 1953. Anion exchange studies. VI. The divalent transition elements manganese to zinc in hydrochloric acid. Journal of the American Chemical Society 75, 1460-1462.

Lebowitz, E., Richards, P., 1974. Radionuclide generator systems, Seminars in nuclear medicine. Elsevier, pp. 257-268.

Mathias, C.J., Welch, M.J., Raichle, M.E., Mintun, M.A., Lich, L.L., McGuire, A.H., Zinn, K.R., John, E.K., Green, M.A., 1990. Evaluation of a potential generator-produced PET tracer for cerebral perfusion imaging: single-pass cerebral extraction measurements and imaging with radiolabeled Cu-PTSM. Society of Nuclear Medicine 31, 351-359.

Qaim, S.M., 2011. Development of novel positron emitters for medical applications: nuclear and radiochemical aspects. Radiochimica Acta 99, 611-625.

Qaim, S.M., 2012. The present and future of medical radionuclide production. Radiochimica Acta 100, 635-651.

Rayner-Canham, G., Overton, T., 2003. Descriptive inorganic chemistry. Macmillan.

Robinson Jr, G.D., Zielinski, F.W., Lee, A.W., 1980. The zinc-62/copper-62 generator: A convenient source of copper-62 for radiopharmaceuticals. The International Journal of Applied Radiation and Isotopes 31, 111-116.

Rowshanfarzad, P., Sabet, M., Reza Jalilian, A., Kamalidehghan, M., 2006. An overview of copper radionuclides and production of 61Cu by proton irradiation of natZn at a medical cyclotron. Applied Radiation and Isotopes 64, 1563-1573.

Schiepers, C., Hoh, C.K., 2006. FDG-PET Imaging in Oncology, Diagnostic Nuclear Medicine. Springer, pp. 185-204.

Shleien, B., Terpilak, M.S., 1992. The health physics and radiological health handbook.

Smith, R.M., Martell, A.E., 1975. Critical stability constants. Springer US.

Soppera, N., Bossant, M., Dupont, E., 2014. JANIS 4: an improved version of the NEA java-based nuclear data information system. Nuclear Data Sheets 120, 294-296.

Turner, J.E., 2008. Atoms, radiation, and radiation protection. John Wiley & Sons.

Yamamoto, Y.L., 1984. Positron emission tomography. Radiation Physics and Chemistry 24, 385-403.

Yokoyama, A., Hosotani, T., Arano, Y., Horiuchi, K., 1986. Development of neutral and bifunctional radiopharmaceuticals using 62Cu-dithiosemicarbazone (DTS) chelate-basic studies on 64Cu chelates. Radioisotopes 35, 249-255.

Ziegler, J.F., 2004. SRIM-2003. Nuclear Instruments and Methods in Physics Research 219, 1027-1036.

Zweit, J., Zweit, R., Goodall, M., Cox, J., Babich, G., Potter, H., Sharma, R., 1992. Development of a high performance zinc-62/copper-62 radionuclide generator for positron emission tomography. European Journal of Nuclear Medicine 19, 418-425.

APPENDIX A

MATLAB FUNCTIONS FOR PRODUCTION YIELD, DOSE RATE, AND COOL

DOWN PERIOD CALCULATIONS.

```matlab
function MainFunction()

%************************************************************%
%*******PARAMETERS TO BE ADJUSTED FOR CALCULATIONS********%
beamCurrent = 25; %uA
n = (6.022E23/63.546); %Describes Target Thickness [atoms/g]
I = (beamCurrent*1E-6)/1.602E-19; %Beam Current for 1 uA [1/s]
time = 1; %Irradiation Time [Hr]
thickness = 1.0; %Target Thickness [mm]
Ei = [18,19,20,21,22,23,24,25,26,27,28,29,30]; %Range of entry energies
[MeV]
leadThickness = 5; %Lead Shielding Thickness [cm]
distance = 100; %Distance measured from point source [cm]
federalLimit = 20; %Federal Regulatory Limit of uSv/Hr
%************************************************************%
%************************************************************%

%Stopping power was taken from SRIM
%StpPwr for Copper
enStpPwr = xlsread('CopperStpPwr.xlsx','A1:A92');%[MeV]
StpPwr = xlsread('CopperStpPwr.xlsx','B1:B92');%[MeV-cm^2/g]

%Energy and Cross Section columns for each radionuclide in the excel
spread sheet.
%Cross Sections were taken from JANIS. TENDL 2013
%Ordered by the following: Zn-62, Zn-63, Zn-61, Cu-61, Co-58, Zn-65,
Cu-64
energy_column = {'A2:A46', 'C2:C46', 'E2:E46',
'G2:G46','I2:I46','K2:K46','M2:M46'};
cs_column =
{'B2:B46','D2:D46','F2:F46','H2:H46','J2:J46','L2:L46','N2:N46'};

%Mass Attenuation Factors for Tissue, taken from NIST
enTissue = xlsread('tissueattenuationfactors.xlsx','A1:A44'); %[MeV]
attenuationTissue = xlsread('tissueattenuationfactors.xlsx','B1:B44');
%[cm^2/g]

%Linear Attenuation Factors for Lead, taken from NIST
enLead = xlsread('leadattenuationfactors.xlsx','A1:A49'); %[MeV]
attenuationLead = xlsread('leadattenuationfactors.xlsx','B1:B49');
%[cm^-1]

%Spline function interpolates a value (CrsSec/StpPwr)
```

```matlab
%From an energy value input. Use
ppval(Function_Name,Projectile_Energy).
FStpPwr = spline(enStpPwr, StpPwr);

%Spline function interpolates a value from an energy input. Returns an
%attenuation value for tissue.
FTissue = spline(enTissue,attenuationTissue);
FLead = spline(enLead,attenuationLead);


zinc_sixtytwo_en = xlsread('EnergyAndYield.xlsx','A3:A33');
zinc_sixtytwo_y = xlsread('EnergyAndYield.xlsx','B3:B33');


zinc_sixtythree_en = xlsread('EnergyAndYield.xlsx','C3:C68');
zinc_sixtythree_y = xlsread('EnergyAndYield.xlsx','D3:D68');


zinc_sixtyone_en = xlsread('EnergyAndYield.xlsx','E3:E48');
zinc_sixtyone_y = xlsread('EnergyAndYield.xlsx','F3:F48');


cop_sixtyone_en = xlsread('EnergyAndYield.xlsx','G3:G33');
cop_sixtyone_y = xlsread('EnergyAndYield.xlsx','H3:H33');


cob_fiftyeight_en = xlsread('EnergyAndYield.xlsx','I3:I5');
cob_fiftyeight_y = xlsread('EnergyAndYield.xlsx','J3:J5');


zinc_sixtyfive_en = xlsread('EnergyAndYield.xlsx','K3:K5');
zinc_sixtyfive_y = xlsread('EnergyAndYield.xlsx','L3:L5');


cop_sixtyfour_en = xlsread('EnergyAndYield.xlsx','M3:M3');
cop_sixtyfour_y = xlsread('EnergyAndYield.xlsx','N3:N3');



%Decay constant
%Ordered by the following: Zn-62, Zn-63, Zn-61, Cu-61, Co-58, Zn-65,
Cu-64
decayConstant = [7.54E-2, 1.08, 28, 2.08E-1, 4.07E-4, 1.183E-4, 5.46E-
2]; %[h^-1]


%For loop that calculates the front term of the production rate
equation
%for each radionuclide.
%Ordered by the following: Zn-62, Zn-63, Zn-61, Cu-61, Co-58, Zn-65,
Cu-64
for i=1:7
    frontTerm(i) = n*I*(1-exp(-decayConstant(i)*time));
end

for j=1:length(Ei)
    %Function energyDeposition calculates the rate of energy loss of
projectile
```

```matlab
    %as it travels through the target, with inputs: initial energy and
target
    %thickness, and returns the values to an array enDep.
    enDep = energyDeposition(Ei(j),thickness);

    %Loop that calculates the energy difference between the energy
    %deposited every 30 microns in the target
    for i = 1:length(enDep)-1
        enDiff(i) = enDep(i)-enDep(i+1);
    end

    %Loop that calculates the Zn-62 production yield for each energy
fraction
    %Also calculates the production of the listed impurities.
    %Ordered by the following: Zn-62, Zn-63, Zn-61, Cu-61, Co-58, Zn-
65, Cu-64
    for i=1:7
        sum = 0; %Initialize
        %Load the energy and cross section from spreadsheet
        en =
xlsread('ReactionCrossSections.xlsx',char(energy_column(i)));%[MeV]
        CrsSec =
xlsread('ReactionCrossSections.xlsx',char(cs_column(i)));%[cm^2]
        %Setup a spline function to interpolate a cross-section for
each energy
        %of the proton as it travels through the copper target.
        FCrsSec = spline(en, CrsSec);
            %Second loop that calculates the yield at each section of
energy
            %deposition and then adds the value to each previous value
            %calculated. This is the equivalent of performing the
integral over
            %the entire cross-section curve.
            for k = 1:length(enDep)-1;
                %Calculates the cross section times difference between
the
                %energy being deposited in each section.
                a = ppval(FCrsSec,enDep(k))*enDiff(k); %[MeV-cm^2]
                %Calculates the stopping power for the proton with a
given
                %energy at each section
                b = ppval(FStpPwr,enDep(k)); %[MeV-cm^2/g]
                %c is the production yield calculated.
                c = ((frontTerm(i)*a)/b); %[Bq]
                sum = sum + c;
            end
            %Error checking to ensure that the yield was calculated
correctly.
            if sum > 0
                ProductionYield(j,i) = (sum/1E6)/(beamCurrent*time);
%[MBq/uA-h]
            elseif sum < 0
```

```
                    ProductionYield(j,i) = 0;
            end
    end

%    Calculating the dose rate for each radionuclide at a distance r
away
%    from a point source gamma emitter at end of bombardment (EOB).
Each
%    individual dose rate is then summed to acquire a total dose rate
for
%    the entire target at a distance r. This is done for every single
%    initial energy selected in the array previously.
%
*********************************************************************
%    NOTE: The dose rate is converted from Rad to Rem assuming a
quality
%    factor of 1 for gamma-rays.
%
*********************************************************************

    sum = 0;
    %Calculating dose rate for Zinc-62
    for i=1:length(zinc_sixtytwo_en)
        energy = zinc_sixtytwo_en(i);
        yield = zinc_sixtytwo_y(i);
        mu = ppval(FLead,energy);
        mfp = mu*leadThickness;
        B = Buildup(energy,mfp);
        if B<0
            B=1;
        end
        sum = sum +
((ProductionYield(j,1)*beamCurrent*1E6*time*yield*energy)/(4*pi()*dista
nce^2))*ppval(FTissue,energy)*B*exp(-mfp)*0.577; %[uSv/hr]
    end
    doseRate(j,1) = sum

    sum = 0;
    %Calculating dose rate for Zinc-63
    for i=1:length(zinc_sixtythree_en)
        energy = zinc_sixtythree_en(i);
        yield = zinc_sixtythree_y(i);
        mu = ppval(FLead,energy);
        mfp = mu*leadThickness;
        B = Buildup(energy,mfp);
        if B<0
            B=1;
        end
        sum = sum +
((ProductionYield(j,2)*beamCurrent*1E6*time*yield*energy)/(4*pi()*dista
nce^2))*ppval(FTissue,energy)*B*exp(-mfp)*0.577; %[uSv/hr]
    end
```

```matlab
    doseRate(j,2) = sum


    sum = 0;
    %Calculating dose rate for Zinc-61
    for i=1:length(zinc_sixtyone_en)
        energy = zinc_sixtyone_en(i);
        yield = zinc_sixtyone_y(i);
        mu = ppval(FLead,energy);
        mfp = mu*leadThickness;
        B = Buildup(energy,mfp);
        if B<0
            B=1;
        end
        sum = sum +
((ProductionYield(j,3)*beamCurrent*1E6*time*yield*energy)/(4*pi()*dista
nce^2))*ppval(FTissue,energy)*B*exp(-mfp)*0.577; %[uSv/hr]
    end
    doseRate(j,3) = sum


    sum = 0;
    %Calculating dose rate for cu-61
    for i=1:length(cop_sixtyone_en)
        energy = cop_sixtyone_en(i);
        yield = cop_sixtyone_y(i);
        mu = ppval(FLead,energy);
        mfp = mu*leadThickness;
        B = Buildup(energy,mfp);
        if B<0
            B=1;
        end
        sum = sum +
((ProductionYield(j,4)*beamCurrent*1E6*time*yield*energy)/(4*pi()*dista
nce^2))*ppval(FTissue,energy)*B*exp(-mfp)*0.577; %[uSv/hr]
    end
    doseRate(j,4) = sum


    sum = 0;
    %Calculating dose rate for Co-58
    for i=1:length(cob_fiftyeight_en)
        energy = cob_fiftyeight_en(i);
        yield = cob_fiftyeight_y(i);
        mu = ppval(FLead,energy);
        mfp = mu*leadThickness;
        B = Buildup(energy,mfp);
        if B<0
            B=1;
        end
        sum = sum +
((ProductionYield(j,5)*beamCurrent*1E6*time*yield*energy)/(4*pi()*dista
nce^2))*ppval(FTissue,energy)*B*exp(-mfp)*0.577; %[uSv/hr]
    end
    doseRate(j,5) = sum
```

```matlab
    sum = 0;
    %Calculating dose rate for Zn-65
    for i=1:length(zinc_sixtyfive_en)
        energy = zinc_sixtyfive_en(i);
        yield = zinc_sixtyfive_y(i);
        mu = ppval(FLead,energy);
        mfp = mu*leadThickness;
        B = Buildup(energy,mfp);
        if B<0
            B=1;
        end
        sum = sum +
((ProductionYield(j,6)*beamCurrent*1E6*time*yield*energy)/(4*pi()*dista
nce^2))*ppval(FTissue,energy)*B*exp(-mfp)*0.577; %[uSv/hr]
    end
    doseRate(j,6) = sum

    sum = 0;
    %Calculating dose rate for Cu-64
    for i=1:length(cop_sixtyfour_en)
        energy = cop_sixtyfour_en(i);
        yield = cop_sixtyfour_y(i);
        mu = ppval(FLead,energy);
        mfp = mu*leadThickness;
        B = Buildup(energy,mfp);
        if B<0
            B=1;
        end
        sum = sum +
((ProductionYield(j,7)*beamCurrent*1E6*time*yield*energy)/(4*pi()*dista
nce^2))*ppval(FTissue,energy)*B*exp(-mfp)*0.577; %[uSv/hr]
    end
    doseRate(j,7) = sum

    sum = 0;
    for i = 1:7
        sum = sum + doseRate(j,i);
    end
    doseRate(j,8) = sum;

    %Initialize the amount of time that the target is left to sit and
    %decay.
    waitTime = 0; %hours
    %Initializing total dose rate of target to use as a comparison to
see
    %if the dose rate of the target is below federally regulated
limits.
    initialDoseRate = doseRate(j,8);
    %While loop that determines how many hours must past before the
doseRate
    %is less than the federally regulated limit, in mRem/hr. Works by
```

90

```matlab
    %increasing the wait time in increments of 1 hour.
    while initialDoseRate > federalLimit
        sum = 0;
        waitTime = waitTime + 1;
        for i=1:7
            sum = sum + doseRate(j,i)*exp(-decayConstant(i)*waitTime);
%[mRem/hr]
        end
        initialDoseRate = sum;
    end
    doseRate(j,9) = waitTime; %Hours

    %Calculate the new production yield for each radionuclide after
decay
    %correcting using the previously calculated wait time.
    for i=1:7
        WaitProductionYield(j,i) = ProductionYield(j,i)*exp(-
decayConstant(i)*waitTime);
    end
end

%Saves the Production yield, the dose rate/total dose rate and wait
time,
%and decay corrected production yields after the wait time has passed
to
%three separate text files with their respective names.
dlmwrite('ProductionYields.txt', ProductionYield);
dlmwrite('DoseRates.txt', doseRate);
dlmwrite('CooldownProductionYields.txt',WaitProductionYield);

end

function [enDep] = energyDeposition(Ei,thickness)

%Range values obtained from SRIM nuclear code
%energy for copper [MeV]
energy =
[0.0,0.011,0.012,0.013,0.014,0.015,0.016,0.017,0.018,0.02,0.0225,0.025,
0.0275,0.03,0.0325,0.035,0.0375,0.04,0.045,0.05,0.055,0.06,0.065,0.07,0
.08,0.09,0.1,0.11,0.12,0.13,0.14,0.15,0.16,0.17,0.18,0.2,0.225,0.25,0.2
75,0.3,0.325,0.35,0.375,0.4,0.45,0.5,0.55,0.6,0.65,0.7,0.8,0.9,1,1.1,1.
2,1.3,1.4,1.5,1.6,1.7,1.8,2,2.25,2.5,2.75,3,3.25,3.5,3.75,4,4.5,5,5.5,6
,6.5,7,8,9,10,11,12,13,14,15,16,17,18,20,22.5,25,27.5,30,32.5,35,37.5,4
0,45,50];
%range for copper [microns]
range =
[0.061,0.0668,0.0726,0.0783,0.084,0.0896,0.0952,0.1007,0.1062,0.1171,0.
1306,0.1438,0.1569,0.1699,0.1827,0.1954,0.2081,0.2206,0.2454,0.27,0.294
3,0.3185,0.3424,0.3663,0.4138,0.4612,0.5084,0.5557,0.6031,0.6506,0.6985
,0.7466,0.795,0.8438,0.893,0.9927,1.12,1.25,1.38,1.52,1.66,1.8,1.95,2.1
,2.41,2.74,3.07,3.43,3.79,4.17,4.97,5.82,6.72,7.67,8.66,9.72,10.81,11.9
6,13.15,14.38,15.66,18.35,21.94,25.79,29.88,34.23,38.81,43.63,48.68,53.
```

```matlab
96,65.18,77.29,90.26,104.08,118.73,134.2,167.51,203.96,243.47,285.99,33
1.45,379.79,430.98,484.97,541.72,601.19,663.35,795.54,975.32,1170,1380,
1610,1850,2110,2380,2660,3270,3930];

%Give this value an energy to spit out the range
FRange = spline(energy, range);

%Give this value an range to spit out the energy
FEnergy = spline(range, energy);

%Target Thickness in units of mm to microns [microns]
targetThickness = thickness*1e3;
%Calculate the range of the particle after it exits particle
exitRange = ppval(FRange,Ei)-targetThickness;
if exitRange < 0
    Ef = 0;
else
    %Calculate the energy of particle from its exit range
    Ef = ppval(FEnergy,exitRange);
end

%Initializing values. All of these values are simply used to correct
record
%All values and make sure that they are all recorded within the correct
%array sizes.
plot_range(1,1) = 0; %Track range
%Track energy deposition, initialize first element with entry energy
enDep(1,1) = Ei;
%Start i at 2, because the first element of the array is initialized
i = 2;
%Track the proton energy deposition in copper in increments of 30
microns
increment = 30;
%Initialize the first element of the array to 0, since zero energy
transfer
%has occured at this point.
dE(i,1) = 0;

%While loop that continues until the protons exits the target. This is
pre-
%determined by the target thickness, which calculates an exit or final
%energy. Once Ei is less than Ef, that designates that the proton has
%exited the target and the loop exits.
while Ei > Ef
    range_value = ppval(FRange,Ei); %enter an energy value, interpolate
a range
    dr = range_value - increment; %## micron increment
    E = ppval(FEnergy, dr); %enter a range value, interpolate an energy
    enDep(i,1) = E; %Keep track of all the E values after energy is
deposited
    %Error checking. See if current E is greater the final E
    %If yes, then do this.
```

```matlab
    if E > Ef
        dE(i,1) = Ei - E; %Keep track of energy deposited
        plot_range(i,1) = plot_range(i-1,1) + increment; %Keep track of
the range of the particle
    %If it's less, then back track in smaller increments of 30 to get a
    %closer estimate of the energy deposited right at the barrier.
    elseif E < Ef
        %Range for whatever is between Ef and last energy
        last_range = ppval(FRange, enDep(i-1,1));
        last_range_2= ppval(FRange, Ef); %range for Ef
        %Add the last little range that is less than the increment
        plot_range(i,1) = plot_range(i-1,1) + (last_range-
last_range_2);
        dE(i,1) = enDep(i-1,1) - Ef;
        enDep(i,1) = Ef;
    end
    Ei = E;
    i = i + 1;
end
```

APPENDIX B

RADIONUCLIDE PRODUCTION AND RADIATION EXPOSURE DATA

Table B-1. Photon energy and yield taken from the NNDC NuDat database.

Zn-62		Cu-61		Zn-65	
Photon Energy	Photon Yield	Photon Energy	Photon Yield	Photon Energy	Photon Yield
(MeV)	$(\gamma \cdot d^{-1})$	(MeV)	$(\gamma \cdot d^{-1})$	(MeV)	$(\gamma \cdot d^{-1})$
0.04	0.25480	0.07	0.04233	1.12	0.50600
0.20	0.00011	0.12	0.00010		
0.24	0.02522	0.22	0.00021		
0.25	0.01898	0.28	0.12200		
0.26	0.01352	0.37	0.02147		
0.30	0.00289	0.53	0.00376		
0.35	0.00450	0.55	0.00006		
0.39	0.00017	0.59	0.01168		
0.49	0.00016	0.66	0.10770		
0.51	0.14820	0.82	0.00307		
0.55	0.15340	0.84	0.00214		
0.60	0.26000	0.90	0.00083		
0.63	0.00001	0.91	0.01102		
0.64	0.00255	0.95	0.00010		
0.64	0.00014	1.02	0.00010		
0.66	0.00001	1.03	0.00042		
0.67	0.00004	1.06	0.00048		
0.73	0.00002	1.07	0.00033		
0.79	0.00009	1.10	0.00245		
0.83	0.00003	1.12	0.00032		
0.88	0.00015	1.13	0.00090		
0.92	0.00015	1.19	0.03747		
1.14	0.00035	1.45	0.00045		
1.19	0.00004	1.54	0.00026		
1.22	0.00002	1.61	0.00021		
1.32	0.00001	1.66	0.00053		
1.39	0.00012	1.73	0.00054		
1.43	0.00028	2.00	0.00004		
1.49	0.00001	2.12	0.00010		
1.53	0.00006	2.12	0.00041		

Table B-1. Photon energy and yield taken from the NNDC NuDat database.

Zn-63				Co-58	
Photon Energy (MeV)	Photon Yield (γ·d⁻¹)	Photon Energy (MeV)	Photon Yield (γ·d⁻¹)	Photon Energy (MeV)	Photon Yield (γ·d⁻¹)
0.24	0.00090	1.55	0.00122	0.81	0.99450
0.37	0.00011	1.57	0.00016	0.86	0.00683
0.44	0.00016	1.67	0.00001	1.67	0.00518
0.45	0.00236	1.70	0.00002		
0.48	0.00006	1.75	0.00004		
0.52	0.00021	1.83	0.00004		
0.58	0.00033	1.86	0.00014		
0.62	0.00014	1.87	0.00020		
0.67	0.08200	2.01	0.00011		
0.68	0.00015	2.03	0.00056		
0.69	0.00004	2.05	0.00004		
0.74	0.00067	2.06	0.00034		
0.75	0.00007	2.08	0.00015		
0.77	0.00007	2.34	0.00075		
0.88	0.00003	2.50	0.00021		
0.90	0.00012	2.51	0.00010		
0.96	0.06478	2.54	0.00066		
1.12	0.00111	2.70	0.00040		
1.13	0.00013	2.72	0.00013		
1.15	0.00019	2.78	0.00016		
1.17	0.00008	2.81	0.00004		
1.21	0.00012	2.86	0.00003		
1.23	0.00002	2.89	0.00002		
1.33	0.00069	3.04	0.00005		
1.34	0.00002	3.10	0.00001		
1.37	0.00034				
1.39	0.00043				
1.39	0.00097				
1.41	0.00746				
1.45	0.00002				
1.48	0.00002				

Table B-1. Photon energy and yield taken from the NNDC NuDat database.

Zn-63				Cu-64	
Photon Energy (MeV)	Photon Yield ($\gamma \cdot d^{-1}$)	Photon Energy (MeV)	Photon Yield ($\gamma \cdot d^{-1}$)	Photon Energy (MeV)	Photon Yield ($\gamma \cdot d^{-1}$)
0.15	0.00172	2.09	0.00628	1.35	0.00473
0.27	0.00546	2.21	0.00842		
0.42	0.00094	2.36	0.00328		
0.43	0.00148	2.38	0.00109		
0.48	0.16850	2.46	0.00655		
0.59	0.00062	2.47	0.00078		
0.60	0.00086	2.54	0.00076		
0.64	0.00078	2.68	0.00679		
0.69	0.01872	2.79	0.00803		
0.70	0.00429	2.84	0.00248		
0.75	0.00312	2.86	0.00429		
0.92	0.00094	2.93	0.00094		
0.93	0.00086	3.02	0.00187		
0.97	0.02574	3.09	0.00117		
1.13	0.00179	3.52	0.00140		
1.15	0.00156				
1.19	0.01724				
1.31	0.00936				
1.39	0.01217				
1.46	0.00312				
1.48	0.00788				
1.50	0.00140				
1.54	0.00085				
1.57	0.00109				
1.61	0.00296				
1.66	0.07800				
1.73	0.00140				
1.88	0.00480				
1.90	0.00091				
1.93	0.00663				
2.00	0.01178				

Table B-2. Linear attenuation coefficients for lead taken from NIST's X-ray and Gamma-ray data section.

Photon Energy (MeV)	μ (cm^{-1})	Photon Energy (MeV)	μ (cm^{-1})
0.001	59081	0.05	91
0.002	14572	0.06	57
0.002	9079	0.08	27
0.003	19573	0.09	22
0.003	22045	0.10	63
0.003	22283	0.15	23
0.003	21058	0.20	11
0.003	20367	0.30	5
0.004	16965	0.40	3
0.004	16352	0.50	2
0.004	14867	0.60	1
0.004	14186	0.80	1
0.005	8283	1.00	0.8
0.006	5298	1.25	0.7
0.008	2593	1.50	0.6
0.010	1481	2.00	0.5
0.013	760	3.00	0.5
0.015	1266	4.00	0.5
0.015	1222	5.00	0.5
0.016	1606	6.00	0.5
0.016	1524	8.00	0.5
0.020	979	10.00	0.6
0.030	344	15.00	0.6
0.040	163	20.00	0.7

Table B-3. Mass energy-absorption coefficients for tissue taken from NIST's X-ray and Gamma-ray data section.

Photon Energy (MeV)	$(\mu/\rho)_{en}$ $(cm^2 \cdot g^{-1})$	Photon Energy (MeV)	$(\mu/\rho)_{en}$ $(cm^2 \cdot g^{-1})$
0.0010	3701	0.06	0.03
0.0010	3376	0.08	0.03
0.0011	3079	0.1	0.03
0.0015	1247	0.2	0.03
0.0020	558	0.2	0.03
0.0021	457	0.3	0.03
0.0023	378	0.4	0.03
0.0025	309	0.5	0.03
0.0026	259	0.6	0.03
0.0028	214	0.8	0.03
0.0030	182	1	0.03
0.0036	106	1.3	0.03
0.0040	80	1.5	0.03
0.0050	41	2	0.03
0.0060	24	3	0.02
0.0080	10	4	0.02
0.0100	5	5	0.02
0.0150	1	6	0.02
0.0200	1	8	0.02
0.0300	0.2	10	0.02
0.0400	0.1	15	0.01
0.0500	0.04	20	0.01

B-4. Proton range in copper for energies between 0.01 and 50 MeV taken from SRIM modeling data.

Proton Energy (MeV)	Proton Range (µm)	Proton Energy (MeV)	Proton Range (µm)	Proton Energy (MeV)	Proton Range (µm)
0.010	0.06	0.17	0.84	3.3	39
0.011	0.07	0.18	0.89	3.5	44
0.013	0.08	0.20	0.99	3.8	49
0.014	0.08	0.23	1.1	4.0	54
0.015	0.09	0.25	1.3	4.5	65
0.016	0.10	0.28	1.4	5.0	77
0.017	0.10	0.30	1.5	5.5	90
0.018	0.11	0.35	1.8	6.0	104
0.020	0.12	0.38	2.0	6.5	119
0.023	0.13	0.40	2.1	7.0	134
0.025	0.14	0.45	2.4	8.0	168
0.028	0.16	0.50	2.7	9.0	204
0.030	0.17	0.55	3.1	10.0	243
0.033	0.18	0.60	3.4	11.0	286
0.035	0.20	0.65	3.8	12.0	331
0.038	0.21	0.70	4.2	13.0	380
0.040	0.22	0.80	5.0	14.0	431
0.045	0.25	0.90	5.8	15.0	485
0.050	0.27	1.00	6.7	16.0	542
0.055	0.29	1.10	7.7	17.0	601
0.060	0.32	1.20	8.7	18.0	663
0.065	0.34	1.30	9.7	20.0	796
0.070	0.37	1.40	11	22.5	975
0.080	0.41	1.50	12	25.0	1170
0.090	0.46	1.60	13	27.5	1380
0.100	0.51	1.70	14	30.0	1610
0.110	0.56	1.80	16	32.5	1850
0.120	0.60	2.00	18	35.0	2110
0.130	0.65	2.25	22	37.5	2380
0.140	0.70	2.50	26	40.0	2660
0.150	0.75	2.75	30	45.0	3270
0.160	0.80	3.00	34	50.0	3930

Table B-5. Reaction cross-sections for the production of relevant radionuclides by bombarding a natural copper target with proton energies between 1 and 200 MeV. This data was taken from JANIS.

Reaction Cross Sections							
Zn-62				Zn-63			
Proton Energy (MeV)	Cross Section (mb)	Proton Energy (MeV)	Cross Section (mb)	Proton Energy (MeV)	Cross Section (mb)	Proton Energy (MeV)	Cross Section (mb)
1	0	28	32	1	0	28	31
2	0	30	24	2	0	30	28
3	0	35	15	3	0	35	21
4	0	40	12	4	0	40	17
5	0	45	9.8	5	129	45	14
6	0	50	8.1	6	233	50	11
7	0	55	6.9	7	276	55	10
8	0	60	6.0	8	293	60	8
9	0	65	5.2	9	310	65	7
10	0	70	4.6	10	326	70	6
11	0	75	4.0	11	339	75	5
12	0	80	3.5	12	348	80	4.6
13	0	90	2.8	13	341	90	3.6
14	3	100	2.2	14	273	100	2.9
15	17	110	1.8	15	192	110	2.3
16	30	120	1.5	16	134	120	1.9
17	40	130	1.3	17	97	130	1.6
18	49	140	1.1	18	75	140	1.4
19	56	150	1.0	19	61	150	1.2
20	60	160	0.9	20	53	160	1.1
22	62	180	0.7	22	44	180	0.9
24	57	200	0.6	24	39	200	0.7

Table B-5. Reaction cross-sections for the production of relevant radionuclides by bombarding a natural copper target with proton energies between 1 and 200 MeV. This data was taken from JANIS.

Reaction Cross Sections							
Zn-61				Cu-61			
Proton Energy (MeV)	Cross Section (mb)	Proton Energy (MeV)	Cross Section (mb)	Proton Energy (MeV)	Cross Section (mb)	Proton Energy (MeV)	Cross Section (mb)
1	0	28	0.02	1	0	28	88
2	0	30	0.31	2	0	30	144
3	0	35	1.76	3	0	35	199
4	0	40	1.77	4	0	40	155
5	0	45	1.15	5	0	45	118
6	0	50	0.83	6	0	50	101
7	0	55	0.68	7	0	55	91
8	0	60	0.57	8	0	60	84
9	0	65	0.49	9	0	65	78
10	0	70	0.43	10	0	70	74
11	0	75	0.38	11	0	75	69
12	0	80	0.33	12	0	80	65
13	0	90	0.26	13	0	90	57
14	0	100	0.22	14	0	100	51
15	0	110	0.18	15	0	110	46
16	0	120	0.16	16	0.01	120	42
17	0	130	0.14	17	0.02	130	38
18	0	140	0.12	18	0.04	140	35
19	0	150	0.11	19	0.08	150	33
20	0	160	0.10	20	0.15	160	30
22	0	180	0.08	22	0.61	180	27
24	0	200	0.07	24	6.86	200	24

Table B-5. Reaction cross-sections for the production of relevant radionuclides by bombarding a natural copper target with proton energies between 1 and 200 MeV. This data was taken from JANIS.

Reaction Cross Sections							
Co-58				Zn-65			
Proton Energy (MeV)	Cross Section (mb)	Proton Energy (MeV)	Cross Section (mb)	Proton Energy (MeV)	Cross Section (mb)	Proton Energy (MeV)	Cross Section (mb)
1	0	28	2	1	0	28	37
2	0	30	7	2	0	30	33
3	0	35	31	3	29	35	25
4	0	40	42	4	133	40	20
5	0	45	37	5	274	45	16
6	0	50	28	6	399	50	13
7	0	55	24	7	489	55	11
8	0	60	22	8	556	60	9.5
9	0	65	26	9	611	65	8.4
10	0	70	34	10	653	70	7.2
11	0	75	44	11	635	75	6.4
12	0	80	54	12	508	80	5.7
13	0	90	64	13	360	90	4.4
14	0	100	64	14	246	100	3.5
15	0	110	61	15	168	110	2.9
16	0	120	56	16	122	120	2.4
17	0	130	54	17	93	130	2.0
18	0	140	52	18	77	140	1.7
19	0	150	48	19	66	150	1.5
20	0	160	48	20	60	160	1.3
22	0	180	44	22	51	180	1.1
24	0.005	200	42	24	46	200	0.9

Table B-5. Reaction cross-sections for the production of relevant radionuclides by bombarding a natural copper target with proton energies between 1 and 200 MeV. This data was taken from JANIS.

Reaction Cross Sections			
Cu-64			
Proton Energy (MeV)	**Cross Section (mb)**	**Proton Energy (MeV)**	**Cross Section (mb)**
1	0	28	324
2	0	30	298
3	0	35	258
4	0	40	234
5	0	45	214
6	0	50	196
7	0	55	177
8	0	60	170
9	0	65	156
10	0	70	148
11	0.02	75	136
12	0.3	80	127
13	6	90	110
14	33	100	95
15	76	110	84
16	124	120	74
17	167	130	67
18	206	140	61
19	241	150	55
20	275	160	51
22	336	180	44
24	365	200	39

Table B-6. The exposure buildup factors for gamma-rays in lead for energies between 0.1 and 10 MeV with relaxation lengths between 0.5 and 10.

MFP	Energy (MeV)									
	10	8	6	5	4	3	2	1	0.5	0.1
0.50	1.28	1.3	1.26	1.25	1.21	1.23	1.21	1.2	1.14	1.51
1.00	1.51	1.51	1.42	1.41	1.36	1.4	1.4	1.38	1.24	2.04
2.00	2.01	1.9	1.73	1.71	1.67	1.73	1.76	1.68	1.39	3.39
3.00	2.63	2.3	2.08	2.05	2.02	2.1	2.14	1.95	1.52	5.6
4.00	3.42	2.91	2.49	2.44	2.4	2.5	2.52	2.09	1.62	9.59
5.00	4.45	3.59	2.96	2.88	2.82	2.93	2.91	2.43	1.71	17
6.00	5.73	4.41	3.51	3.38	3.28	3.4	3.32	2.66	1.8	30.6
7.00	7.37	5.39	4.13	3.93	3.79	3.89	3.74	2.89	1.88	54.9
8.00	9.44	6.58	4.84	4.56	4.35	4.41	4.17	3.1	1.95	94.7
10.00	15.4	9.73	6.61	6.03	5.61	5.56	5.07	3.51	2.1	294

APPENDIX C

LABVIEW PROGRAM LOGIC FLOW DIAGRAMS
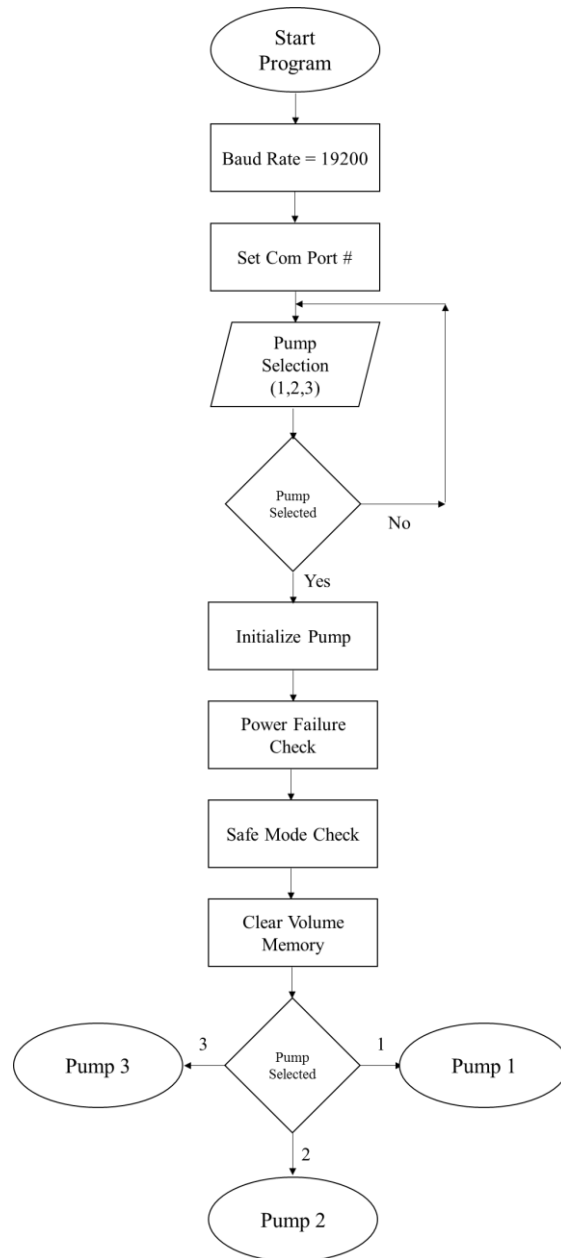
Figure C-1. Logic flow diagram for the LabVIEW program developed for the NE-500
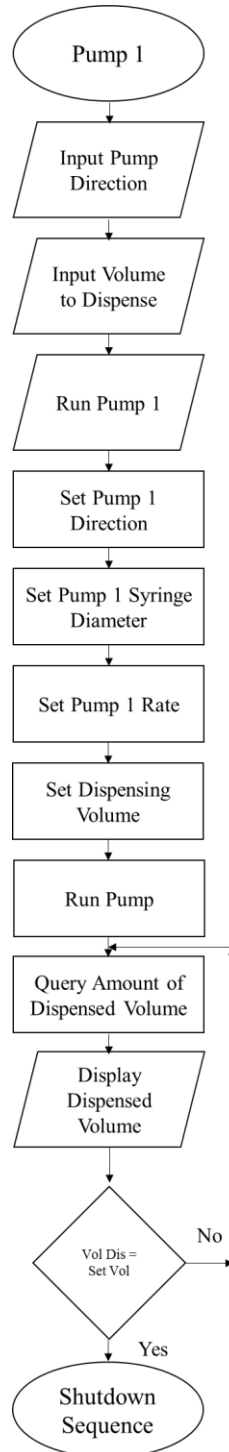
Figure C-2. Logic flow diagram for controlling pump 1 with the LabVIEW program developed for the NE-500
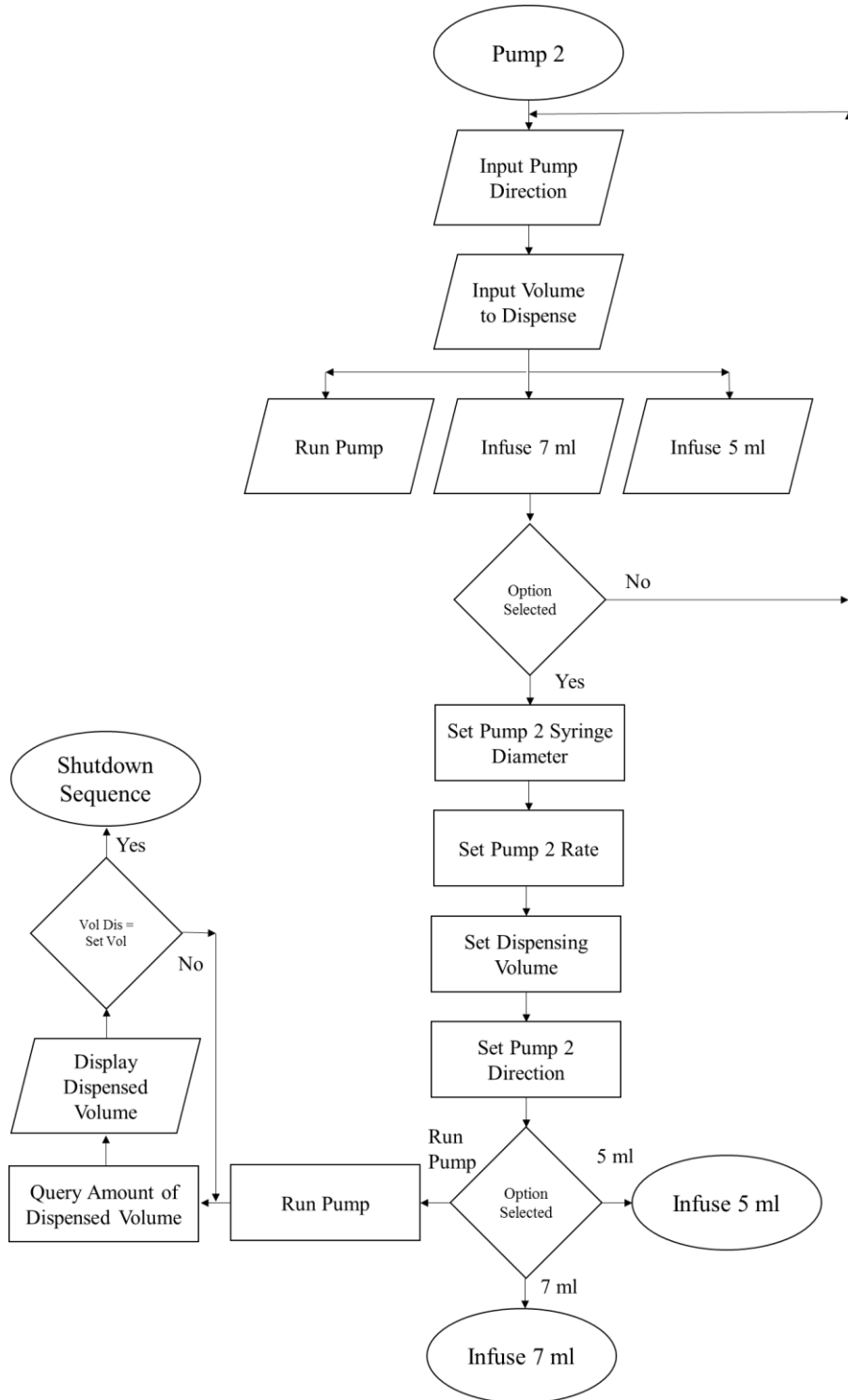
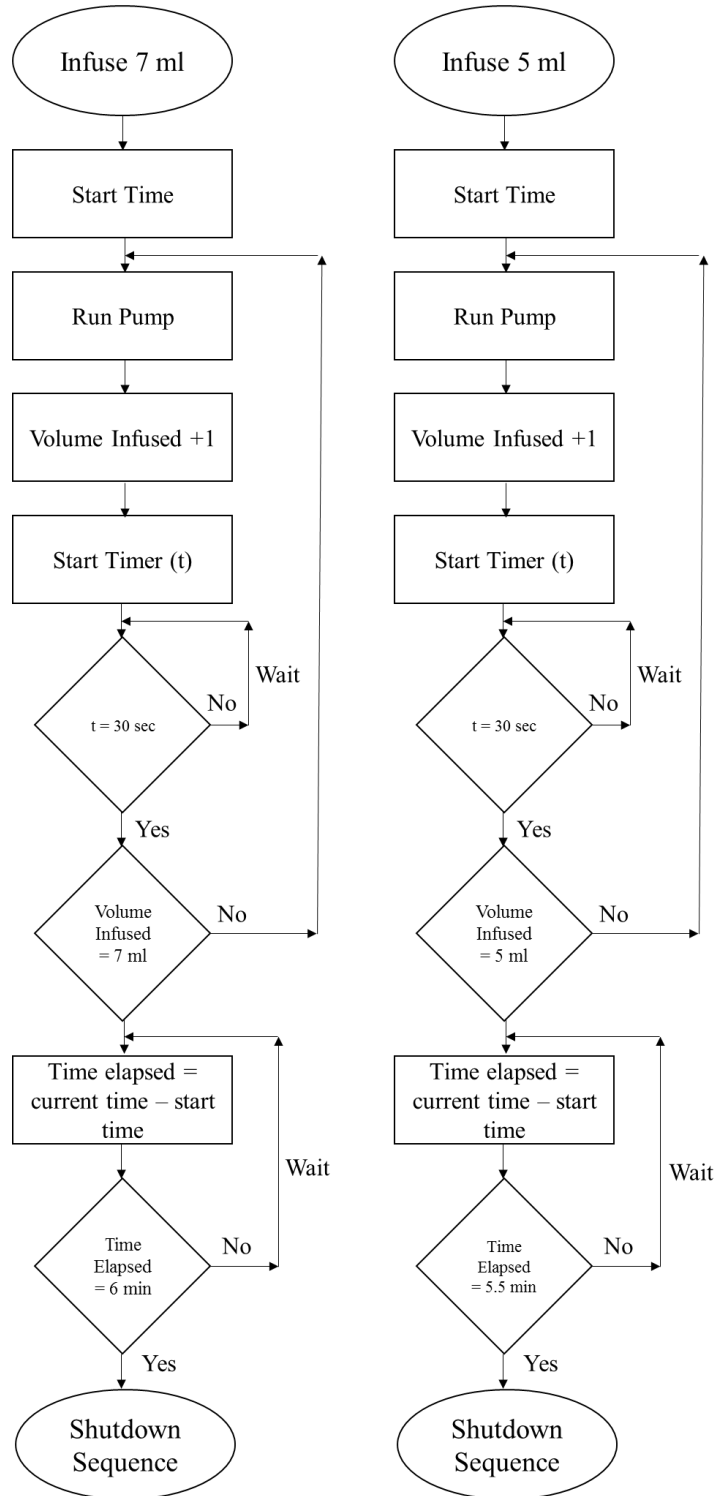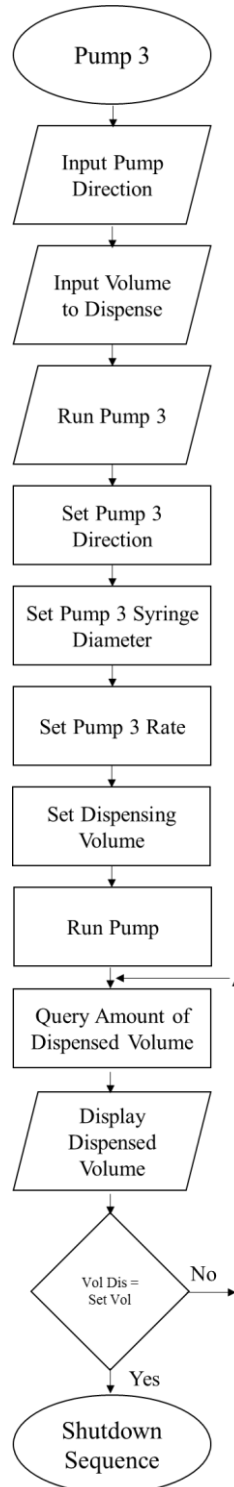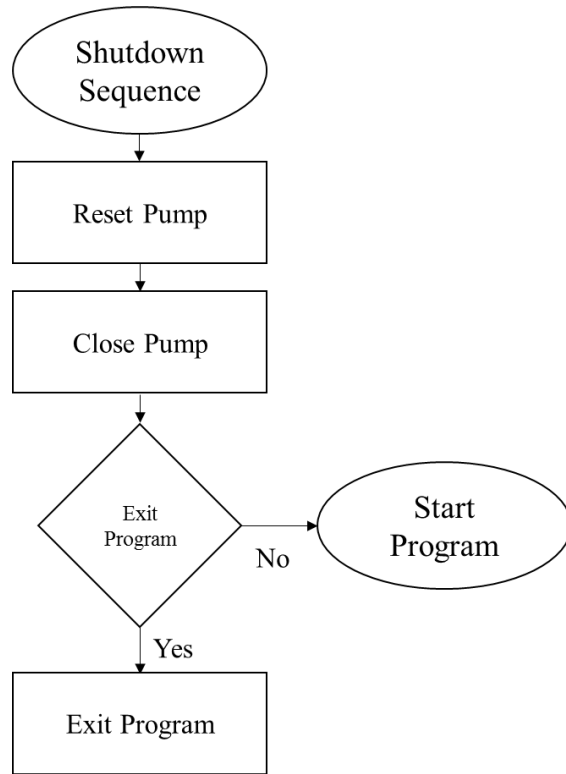Figure C-3. Logic flow diagram for controlling pump 2 with the LabVIEW program developed for the NE-500

Figure C-4. Logic flow diagram for automating the addition of hydrogen perxoide using pump 2 with the LabVIEW program developed for the NE-500

Figure C-5. Logic flow diagram for controlling pump 3 with the LabVIEW program developed for the NE-500

Figure C-6. Logic flow diagram for close down the program developed for the NE-500
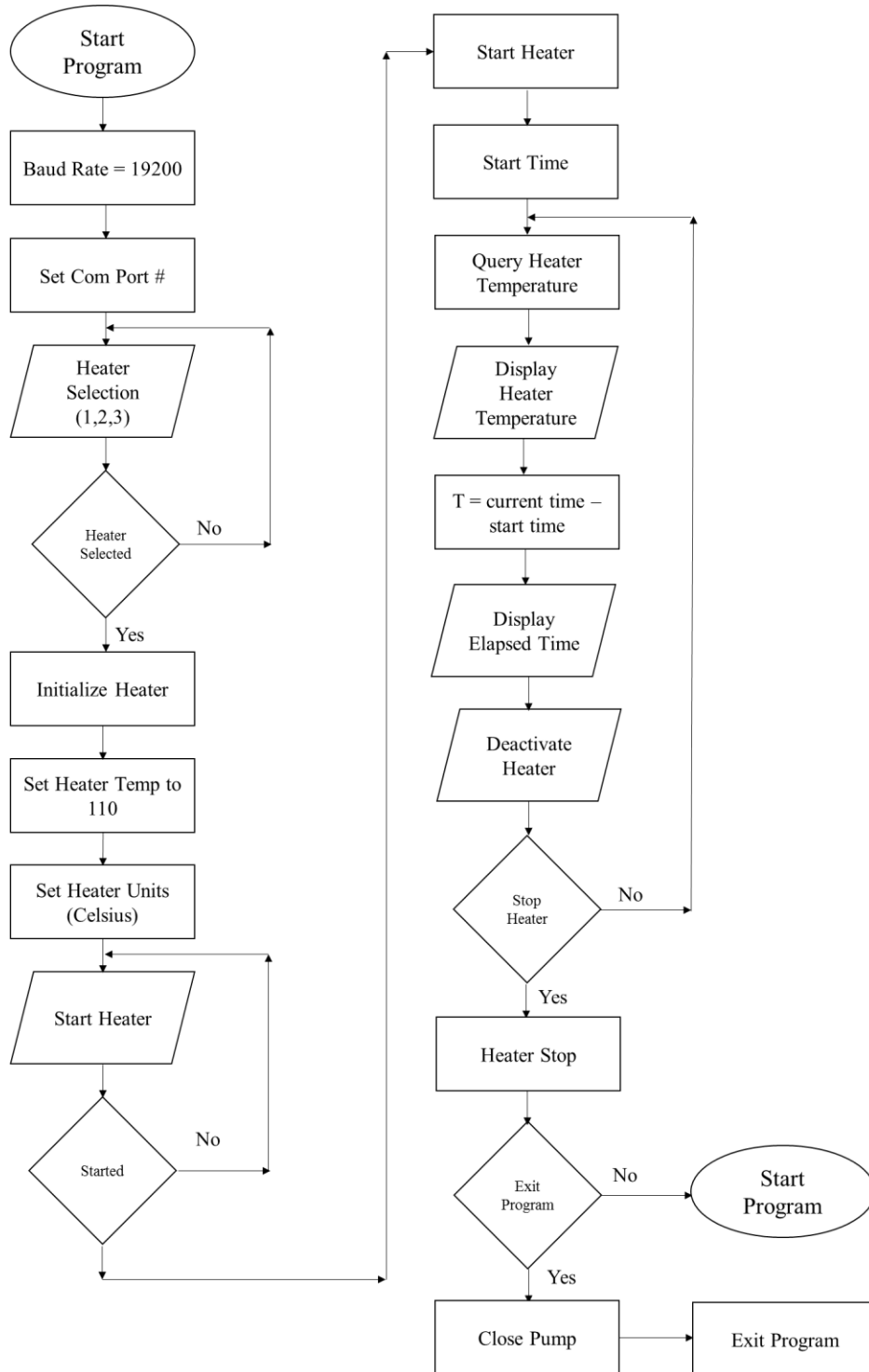
Figure C-7. Logic flow diagram for the LabVIEW program developed for the HEATER-KIT-1LG.
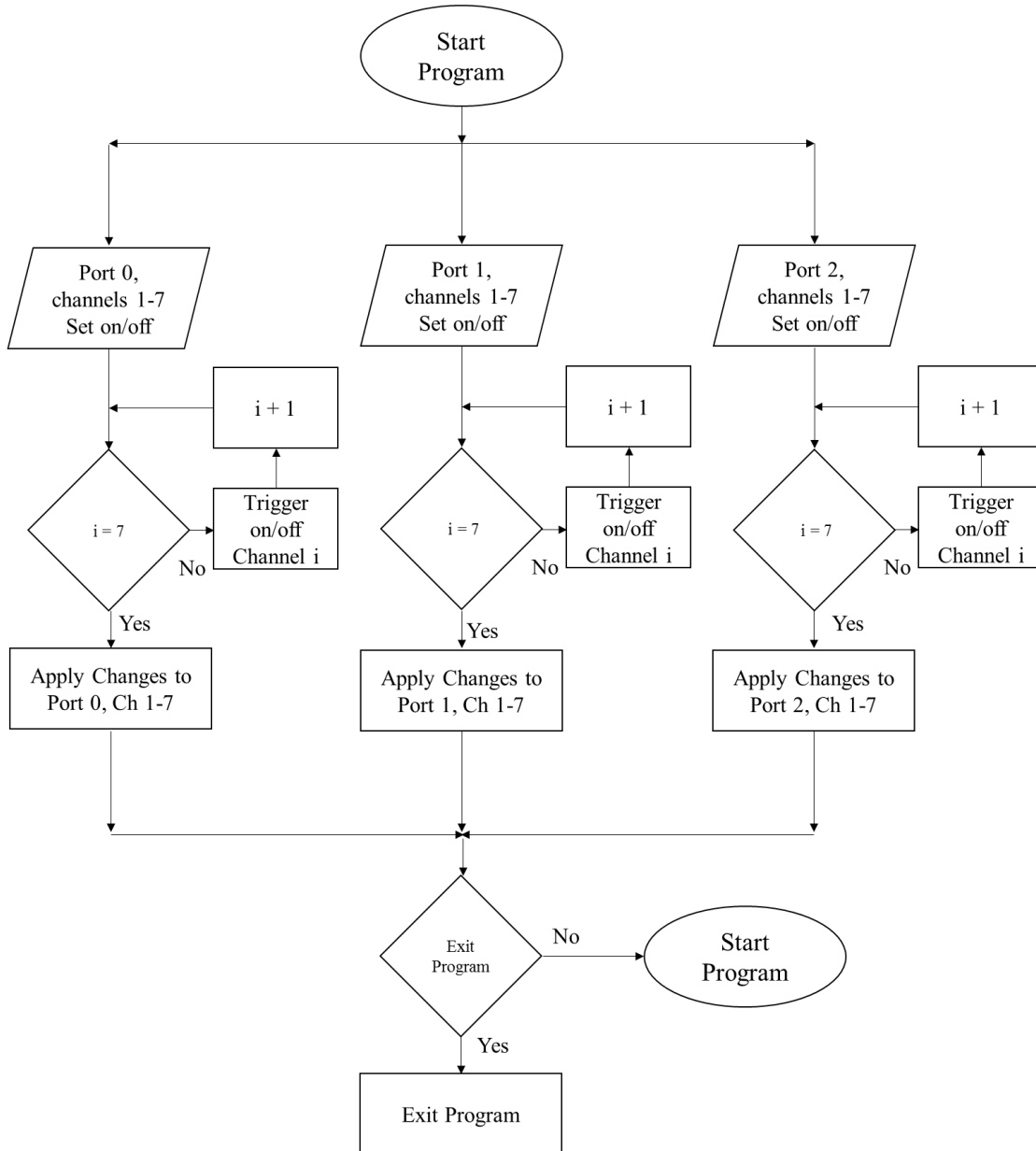
Figure C-8. Logic flow diagram for the LabVIEW program developed for the USB-6501.
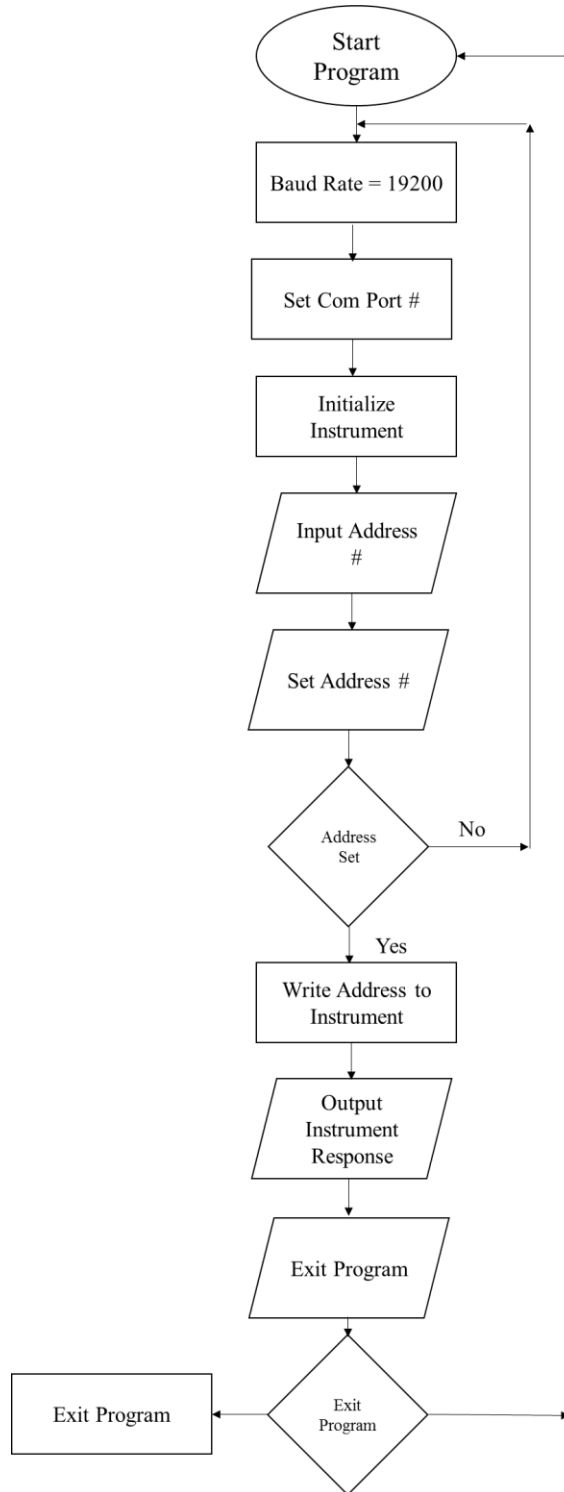
Figure C-9. Logic flow diagram developed for the LabVIEW program that manually sets the address of an instrument.